Chapter 18
Industrial Applications of Terahertz Imaging

J. Axel Zeitler and Yao-Chun Shen

Abstract This chapter gives a concise overview of potential industrial applications for terahertz imaging that have been reported over the past decade with a discussion of the major advantages and limitations of each approach. In the second half of the chapter we discuss in more detail how terahertz imaging can be used to investigate the microstructure of pharmaceutical dosage forms. A particular focus in this context is the nondestructive measurement of the coating thickness of polymer coated tablets, both by means of high resolution offline imaging in research and development as well as for in-line quality control during production.

18.1 Introduction

The advent of terahertz time-domain technology has brought with it a keen interest in its use in imaging experiments [1–3]. A number of imaging application examples have been reported: metal contacts of a packaged integrated circuit chip, as well as the leaf structure of plants [1]; polymer composites and flames [2]; breakfast cereals and chocolate [4]; tree-ring analysis [5]; medical tissues (see Chap. 16 by MacPherson in this book); analysis of polymer samples [6] and pharmaceutical tablets [7–9], among many other examples. A number of reviews and book chapters have summarised the recent progress in terahertz imaging [4, 6, 10–19]. However, despite the interesting

J. A. Zeitler (✉)
Department of Chemical Engineering and Biotechnology,
University of Cambridge, CambridgeCB2 3RA, UK
e-mail: jaz22@cam.ac.uk

Y.-C. Shen
Department of Electrical Engineering and Electronics,
University of Liverpool, Brownlow Hill, LiverpoolL69 3GJ, UK
e-mail: y.c.shen@liverpool.ac.uk

K.-E. Peiponen et al. (eds.), *Terahertz Spectroscopy and Imaging*,
Springer Series in Optical Sciences 171, DOI: 10.1007/978-3-642-29564-5_18,
© Springer-Verlag Berlin Heidelberg 2013

results introduced by all these studies, only a select few applications show industrial promise or have already been successfully demonstrated in an industrial setting.

This chapter briefly highlights some potential areas of industrial application and then focuses specifically on applications in the pharmaceutical industry, a field that shows great promise for industrial terahertz applications.

18.2 Industrial Imaging

18.2.1 General Principles

In order to exploit the unique properties of terahertz radiation for imaging applications in an industrial context commercial imaging technology is required. The instruments need to be rugged and robust enough to operate in an industrial manufacturing environment, while at the same time providing sufficient sensitivity to measure the required process parameters. The cost and reliability of the equipment are further critical factors and, most importantly, there needs to be a compelling case in terms of economic benefits to industry to invest in this relatively young technology rather than the more established measurement sensors.

In one of the first reviews on terahertz imaging more than 15 years ago, Mittleman, Jacobsen and Nuss provided a compelling case for using terahertz technology for the quality control of polymer materials [2]:

> "Detection of [air pockets in polymer foam bonds] is a significant quality control issue, and no simple method currently exists. X-ray transmission does not provide a high contrast between the plastic-rubber foam and the air; in addition, health and safety issues preclude the use of X-ray diagnostics here. Ultrasound analysis is effective only with the use of an index-matching fluid, while other probing techniques such as magnetic resonance imaging are too expensive and cumbersome. Probing the parts with microwaves would work quite nicely, except that it would be difficult to detect voids significantly smaller than the wavelength of the radiation used. Since, in this case, it is desirable to detect voids smaller than one centimetre in diameter, this effectively eliminates conventional microwave analysis from consideration."

In fact, all industrial terahertz imaging applications that have been discussed since are based on this unique combination of high imaging contrast and sufficiently high spatial resolution; as well as inherent safety. Mittleman, Jacobsen and Nuss go on to state that [2]:

> "It should be emphasised that one could detect voids of this sort without relying on [small differences in transmittance] by observing the *transit time* of the terahertz pulse through the material, rather than the transmitted *amplitude*. The combination of the amplitude and phase information measured in THz-TDS make for a very powerful tool for quality control measurements."

The coherent detection scheme together with the resulting time-domain signal of the terahertz pulse lead to the high sensitivity and excellent contrast that can be

achieved in terahertz imaging. This is a major difference to conventional far-infrared technology and it is this property that makes terahertz imaging attractive for industrial applications.

Over the past decade, key developments were initiated by the commercial terahertz equipment manufacturers. During this period the two major drivers in the field were TeraView Ltd. in Cambridge, UK, and Picometrix LLC, Ann Arbor, MI, USA. Both companies have successfully demonstrated new industrial applications, have developed terahertz sensors that can be used in a manufacturing environment and have installed such instruments across a range of industries. At the same time a number of smaller companies have formed and this has greatly accelerated the further development of more robust instrumentation. With the advent of cheaper 800 nm fibre laser technology, an increased interest from more established optics companies and a growing awareness of the potential of terahertz technology by industrial end users, industrial imaging applications have grown considerably.

Most of the studies that have explored the industrial applications of terahertz technology reviewed in this chapter, are proof-of-principle experiments that demonstrate what information terahertz images can reveal. However, there are a few published examples where terahertz sensors were used to measure samples directly under industrial processing conditions. The examples range from the automated imaging of coated pharmaceutical tablets to investigate the thickness and homogeneity of polymer coatings [20]; an in-line sensor that was developed to monitor a polymer compounding process [21]; an in-line thickness gauge to measure the thickness of polymer laminates during production [22]; and an in-line sensor that was demonstrated to measure the thickness of polymer coatings on individual tablets during production [23].

However, in order to establish itself long-term as a complementary imaging technique in nondestructive testing [24–26], terahertz imaging has to further demonstrate how it will add value to currently available technologies. The main competing technologies are X-Ray tomography and imaging; ultrasound testing [27]; infrared thermography; eddy current testing, and optical coherence tomography (OCT) [28].

18.2.2 Contrast Mechanisms

Before we start looking into specific examples of imaging applications we would like to highlight briefly the main physical phenomena that give rise to contrast in terahertz images. The fundamental imaging principles were first described by Mittleman et al. [3] and, for more detail, we would like to refer the reader to the Chap. 17 by Shibuya and Kawase, which provides an excellent introduction to the concept of terahertz pulsed imaging and terahertz tomography. For a good introduction to general terahertz imaging, see Lee [17].

In addition to the standard image signal processing and data analysis techniques, further refinements were developed to improve the extraction of optical constants from transmission measurements of thin single layer samples [29] as well as

multilayered samples [30]. However, other measurement techniques, such as OCT, are more mature and readily suited to measure the thickness of thin samples. For this reason, and due to the limited power that can be generated with the currently available pulsed terahertz sources, most industrial imaging applications are currently performed in reflection mode.

Industrial applications of terahertz imaging will most likely involve the analysis of solid samples that are highly transparent to terahertz radiation and where contrast is achieved either by a change in refractive index, absorption coefficient or scattering.

18.2.2.1 Dielectric Properties and Vibrational Modes

Chapter 8, by Parrott et al., provides an overview of the spectroscopic properties of solids at terahertz frequencies. The main contrast mechanism that is typically exploited in terahertz time-domain reflection, or tomographic, imaging is the difference in refractive index between two materials. In time-domain terahertz imaging the field E of the electromagnetic wave, rather than its intensity, is measured and hence the reflectivity R is

$$R = \frac{|E_{\text{interface}}|^2}{|E_0|^2} = \frac{(n_1 - n_2)^2}{(n_1 + n_2)^2}, \tag{18.1}$$

where $E_{\text{interface}}$ denotes the electric field of the electromagnetic wave of the reflection from the sample interface and E_0 is the reflection from a reference, typically a mirror, and n_1 and n_2 are the refractive indices of the two media that the terahertz pulse is propagating through.

As the terahertz pulse is propagating through the sample a reflection will occur whenever there is a change in refractive index. This change in refractive index can either be due to the propagation of the pulse from one type of material into another or it can be due to a distinct difference in density of the sample matrix which in turn is reflected in a change in optical density.

In most (semi-)transparent materials at terahertz frequencies the refractive index does not change significantly across the frequency components of the terahertz pulse. However, as detailed in Chaps. 7 and 8, in some crystalline materials the intermolecular vibrational modes fall into the terahertz frequency range, and hence pronounced changes in both the absorption coefficient and refractive index can be observed at the distinct frequencies of the vibrational modes.

This change in optical properties can be used to generate contrast in the resulting terahertz images when processing the image data in the frequency domain. It is possible to identify a wide range of small organic molecules [31, 32]; different crystal structures of the same molecule [33–35]; degradation products in polymers [36], and many other types of molecules as outlined in Chap. 8.

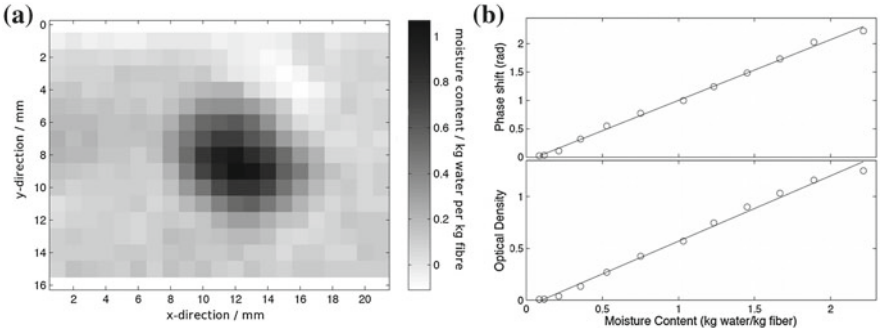

Fig. 18.1 **a** Transmission image through 80 g/m^2 paper at 0.6 THz showing the distribution of water in terms of absolute moisture content; **b** phase change (*upper panel*) and relative optical-density (*lower panel*) relative to the dry paper sample shown as a function of the water content in the moist sample (modified from [37])

18.2.2.2 Polar Liquids / Moisture

The optical properties are not only influenced by differences in density within the sample matrix or vibrational modes but there is also a strong attenuation of the terahertz pulse due to the presence of polar liquids, as outlined in Chaps. 9 and 16.

This effect can be exploited to quantify the amount of moisture in paper [37, 38] (Fig. 18.1), in food [39] or in non-polar liquids such as crude oil [40]. In such applications terahertz techniques were shown to have advantages in detection sensitivity, acquisition speed and much reduced scattering effects when compared to infrared techniques.

18.2.2.3 Conductivity

As outlined in Chap. 8, Sect. 8.4.2 the conductivity σ of the sample is related to the dielectric constants by $\epsilon = \epsilon_\infty + i(\sigma)/(\omega\epsilon_0)$. This means that, with increasing conductivity, both the absorption coefficient and refractive index also increase as $\epsilon = \epsilon' + i\epsilon'' = (n + i\kappa)^2$.

This property can be exploited for the characterisation of the electronic properties of catalysts. Using quantitative physical models it is possible to extract the defect density as well as the graphicity of catalytically active carbon materials such as carbon nanofibres [41]. The same approach can also be used to analyse the electronic properties of hydrocarbons that form on the surface of a catalyst during heterogeneous catalysis. Depending on the reaction conditions, the hydrocarbons can either lead to unwanted deactivation of the catalyst or the carbon structure can play an active role in the catalytic reaction [42–44].

18.2.3 Nondestructive Testing

In the field of non-destructive testing a wide range of materials from different industries has been analysed. Typically, the most successful applications have involved materials that are quite transparent at terahertz frequencies. In the food industry the main applications have been the detection of potential contaminations within a food matrix, such as glass splinters in chocolate [4, 45], or to assess the homogeneity of mixtures, such as raisins and cereal, in a boxed product [4]. In contrast a lot more work has been reported for NDT applications in the fields of polymers and ceramics, both again classes of materials that are mostly transparent at terahertz frequencies.

Starting from the early work by Mittleman et al. [2] on composite plastic parts (Fig. 18.2) the basic imaging concept was applied to image the integrity of the space shuttle fuel tank foam insulation [46]. The authors showed that it is possible to locate voids and disbonds that were intentionally incorporated within a test piece of foam insulation using time-domain terahertz imaging. The study by Picometrix showed that it is possible to use a terahertz sensor that was attached to a 30 m long optical fibre in such imaging applications. A similar study investigating the integrity of polyurethane foam was also reported at the same time by Zhong et al. in collaboration with Lockheed Martin [47]. These studies attracted considerable attention both in the terahertz, as well as the wider NDT community. The technology was subsequently evaluated by NASA for its suitability to detect nondestructively the early onset of corrosion on the metal surface under tiles up to 76 mm of thickness used as part of space shuttle insulation [48]. The authors concluded that terahertz imaging was a unique NDT technique for detecting hidden corrosion under the space shuttle tiles, which was previously considered undetectable when there is only access from one side of the structure. Zimdars et al. showed how the entire volume of samples of Kevlar soft shell fan containment systems, silica thermal protection tiles and sprayed on foam thermal insulation can be analysed using terahertz computed tomography [49].

Chapter 13 by Jansen et al., gives a comprehensive overview of how terahertz radiation can be used to analyse polymers together with selected examples of applications. However, as this chapter is primarily concerned with industrial applications of terahertz imaging, it seems appropriate to highlight a few select studies that fall into this remit. Morita et al. published two studies that demonstrated the ability of terahertz NDT to detect leaks as small as 30–40 μm in plastic packaging materials [50] and how this technique could be used for food applications [51]. Again, the main advantages of the technique highlighted by these two studies, compared to competing technologies such as ultrasound, were that no immersion in matching refractive index liquid is required in THz NDT and that it is suitable to investigate opaque materials. Further examples of potential industrial applications of terahertz imaging are the investigation of the fibre alignment in reinforced plastics [52] and the coating integrity of jet engine turbine blades [53, 54]. A good overall summary of the current state of THz NDT applications recently published by Lopato et al. [55] and Hsu et al. provide some interesting insights into recent developments [56].

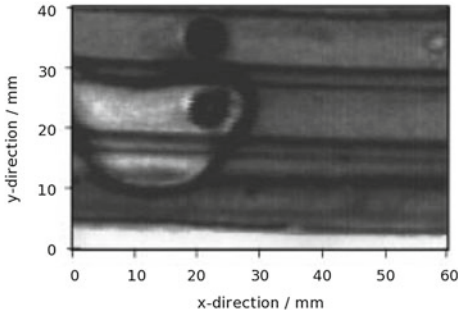

Fig. 18.2 Terahertz image of a moulded composite plastic piece made from two parallel black plastic sheets, with a rubberised foam padding between them. The foam is sprayed between the plastic sheets, holding them together when it dries. The image shows the presence of a defect of roughly 20 mm diameter in the internal foam-filled region on the left of the part (modified from [2])

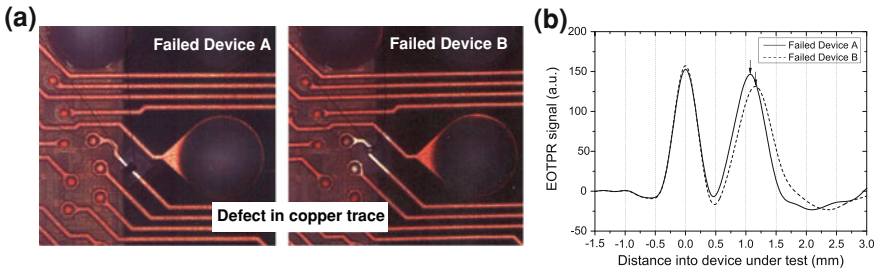

Fig. 18.3 Electro Optical Terahertz Pulse Reflectometry (EOTPR) for semiconductor fault testing. **a** Optical images of the two failed devices showing the cut in the copper traces. **b** Results obtained with EOTPR (source: TeraView Ltd.)

Recently, interest in semiconductor failure testing using pulsed terahertz radiation has rekindled. Very promising results in microelectronic package fault isolation and failure analysis have been reported where the new terahertz instrument shows significant advantages over conventional time-domain reflectometry, both in terms of the resolution that can be achieved as well as the bandwidth and measurement speed [57, 58]. Figure 18.3 shows Electro Optical Terahertz Pulse Reflectometry (EOTPR) results from an accuracy test. Here, the aim was to measure the difference in distance between two cut copper traces in the same circuit of two identical integrated circuit devices. The difference in position of the leading edge of the cut is 89 μm. During operation pulses are launched into the device under test via a high frequency circuit probe. Portions of the pulse are reflected back as it encounters changes in impedance within the integrated circuit such as open or short circuit defects. Reflections are recorded as a function of time and result in the EOTPR waveform. The arrows on plot b) of Fig. 18.3 indicate the reflections due to the cut in the copper traces. The positive reflection indicates that the cut has resulted in an open circuit. The peak posi-

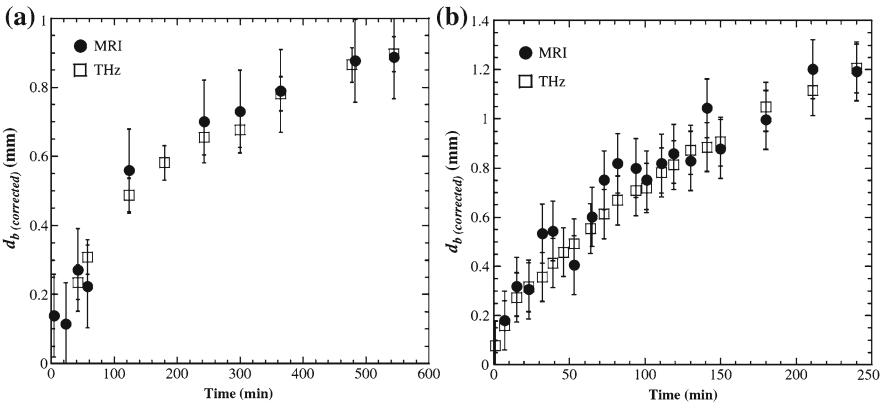

Fig. 18.4 Nondestructive measurement of the penetration front of a solvent (in this case acetone) into different polymers at room temperature: **a** polycarbonate; and **b** polyvinylchloride. The terahertz data was acquired in reflection through the polymer sample. The results were compared to MRI analysis of similar samples and excellent agreement was found (modified from [59])

tion gives the location of the fault and from the location we can obtain the separation between the faults in devices A and B. This example illustrates how EOTPR can be used to identify a fault and determine its location. As this development is driven by the semiconductor industry together with terahertz instrument manufacturers, this field of industrial applications is likely to grow considerably in the coming years.

Another very interesting application of terahertz imaging is the measurement of liquid ingress into polymers as described by Obradovic et al. [59]. Using terahertz reflection imaging it was possible to quantify the ingress of acetone into two samples of polymer (Fig. 18.4). The results of this study suggested that terahertz imaging has the potential to characterise liquid mobility and subsequent conformational changes in the polymer matrix.

Two studies that should be mentioned in the field of polymer analysis in an industrial context are the development of an online polymer compounding sensor that can be used to monitor the compounding process during manufacture [21], and an in-line terahertz measurement gauge that was developed to control the lamination process of a two-layer roofing plastic insulation membrane [22]. The latter study demonstrated that the layer thickness of the laminate can be measured reliably and, at the same time, that delaminations can be detected in real time during process conditions (Fig. 18.5). The work is of particular significance as, rather than as part of a proof-of-principle study, this measurement sensor was installed on the production line of a company. To our knowledge, this is the first time that a terahertz sensor has been endorsed by an industrial end user in this way and put to routine use in a manufacturing environment.

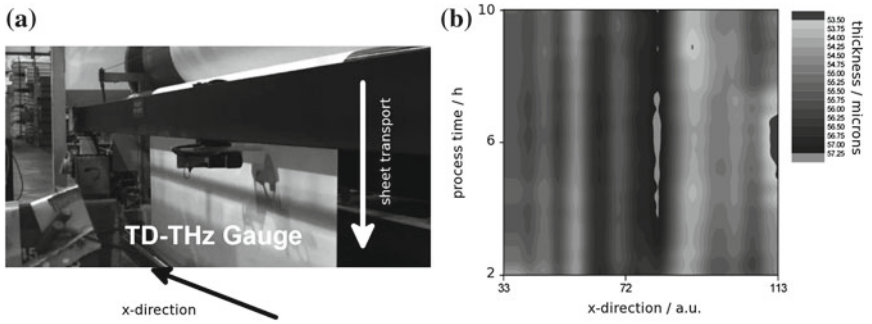

Fig. 18.5 Terahertz gauge mounted on a gantry in the production line of the plastic sheet lamination process. **a** Photograph of the setup; **b** Measurement results over process time. The total thickness of the sheet is represented by different grey values (modified from [22])

18.2.4 Real-Time Imaging

As the previous section shows, there are a number of exciting applications for terahertz imaging in an industrial context. However, from the technology point of view, one considerable limitation is that all imaging experiments have to be performed by raster scanning over the object of interest. The image is mapped out pixel by pixel, which can take anything between a couple of minutes to a couple of hours depending on the size of the object and the spatial resolution required for the particular application. This lack of real-time imaging capability is a genuine limitation of terahertz imaging as it limits the current industrial imaging applications to 1D measurements in process control (e.g. terahertz depth gauge, with process time providing the second dimension) or to offline 2D and 3D measurements with limited throughput in terms of number of samples or size of object that can be analysed.

The first successful demonstration of how to achieve real-time 2D imaging using terahertz radiation was made by Wu et al. [60–62]. For this purpose the same measurement concept that is commonly used in the detection of terahertz pulses in THz-TDS, as outlined in detail in Chap. 1, was used in a 2D configuration rather than in 1D. Using frequency upconversion by means of an electro-optic crystal such as ZnTe it was possible to image the terahertz beam using a CCD focal-plane camera. In this configuration imaging is performed in transmission and the image quality is limited by the low brightness of the commonly used pulsed sources as well as the purity of the ZnTe crystal which limits its applications. However, the advantage of this technology is that the terahertz pulses are inherently broadband, and hence spectral information of the samples can be analysed easily. This imaging concept has been used to discern different chemicals [63, 64], monitoring the drying process of paint [65] and revealing hidden objects in plastic pipes and polymer matrices [66].

Using a gas laser operating at 2.52 THz, Lee and Hu took this 2D imaging concept forward to achieve faster acquisition speeds by utilising a focal plane array detector and exploiting the much higher brightness of the gas laser (10 mW output power

compared to μW power in the time-domain systems), thereby achieving a much better signal-to-noise ratio at frame rates of up to 60 frames per second [67]. They later demonstrated the same imaging principle by using more compact Quantum Cascade Lasers [68] instead of the gas laser [69]. This development potentially opens up new opportunities by utilising QCLs that can be switched between different output frequencies [70] as well as by extending the imaging work to tomography applications [71].

18.3 Pharmaceutical Industry

18.3.1 Specific Imaging Requirements

In the pharmaceutical industry the most commonly used, and most commercially valuable, dosage form for administering a drug to a patient is the tablet. A tablet is a compacted powder designed to be swallowed. Once it reaches the desired site in the gastrointestinal tract—either the stomach, the small intestines or the colon—it will disintegrate. The drug molecules will subsequently dissolve and, once in, solution absorption (typically through the intestinal mucosa) occurs before the drug is distributed throughout the body by blood circulation.

The microstructure, distribution, particle size and morphology of all materials that are part of the tablet formulation, such as the drug molecules and the excipient components, have a strong impact on physical attributes that are important during manufacture. These include tablet hardness, robustness and adhesion to the tablet punch, as well as more chemical characteristics such as the stability of the drug molecules which, in turn, influences the tablet shelf-life and ultimately its bioavailability, i.e. how much of the drug molecules actually reaches the bloodstream.

In recent years solid dosage forms with sophisticated polymer coatings, or insoluble porous matrix structures, have been developed. Such advanced drug delivery techniques have gained more and more importance in order to meet increasing expectations for efficient and controlled drug delivery. This in turn has resulted in more complex processes for the production of such structures, which require exact control to ensure the quality of the resulting product. Consequently, there is a strong demand in the pharmaceutical industry for non-destructive imaging technology to assess the microstructure of the tablet throughout product development and manufacturing in order to ensure its quality while optimising the productivity and, ultimately, profitability.

Various imaging methods have been proposed to assess product performance and quality through evaluating the physical and chemical uniformity within a tablet [8, 72, 73]. Infrared and/or FTIR-Raman imaging are able to reveal the uniformity of drug molecules of a sample (near the surface). However, using this technique, a full 3D chemical map would require slicing through the tablet many times: an approach which is destructive, time-consuming and which may introduce artefacts to the tablet

under investigation. On the other hand, X-ray computed microtomography provides a full high resolution 3D map of the microstructure of a tablet; yet its contrast is limited by the small differences in electron density within a typical formulation (except for inorganic pigments that are used in some coatings). It has thus little or no chemical specificity to differentiate: for example, drug molecules from excipients within a tablet. In addition, the data acquisition and reconstruction is relatively time-consuming and there can be safety concerns when using ionising radiation depending on the environment the instrument is operated within.

As discussed above, the 'ideal' imaging technique should be capable of mapping and analysing the internal structures within complex pharmaceutical products nondestructively. It should be able to reveal structural defects such as coating delamination, capping and cracking inside a tablet, as well as having the ability to map chemical non-uniformities such as a segregation of drug and excipient particles. The technique needs to be non-destructive and non-invasive (leaving the sample intact and in its original state during analysis), accurate and efficient, easy and safe to use.

Imaging of pharmaceutical dosage forms using terahertz radiation is a very attractive option due to the fact that most materials that are used as excipients for tablets are amorphous and hence do not exhibit any distinct spectral features while at the same time they are (semi-)transparent. This makes it possible to carry out non-destructive imaging at depth due to the high penetration depth that can be achieved. On the other hand, most drug molecules are small organic molecular crystals and have distinct vibrational modes at terahertz frequencies (see Chap. 8 by Parrott et al. for further details). This means that not only can drug particles be identified within the tablet matrix but different drug molecules can be distinguished quantitatively.

In subsequent sections we will discuss first the practical aspects of terahertz imaging instrument/measurement in the context of pharmaceutical applications, followed by an overview of some recent application highlights of terahertz imaging in pharmaceutics and solid dosage forms. A number of more detailed technical reviews on pharmaceutical applications of terahertz time-domain spectroscopy and imaging were published recently and the reader is referred to these reviews for any further details that are beyond the scope of this chapter [7, 9, 74, 75].

18.3.2 Instrumentation

To date, the most commonly used terahertz imaging technique for the quantitative characterisation of pharmaceutical solids is terahertz time-domain spectroscopy in reflection, also referred to as terahertz pulsed imaging (TPI) [20, 76]. Figure 18.6 shows the schematic diagram of a typical TPI system (in this case the TPI imaga 2000, TeraView Ltd., Cambridge, UK), which was specifically designed for applications in the pharmaceutical industry. The core technology of the TPI system is based on terahertz generation and detection using an ultrafast laser as described in Chap. 1 of this book by Freeman et al. In brief, a beam splitter separates the near-infrared laser light into an excitation beam and a probe beam. Terahertz pulses are generated by

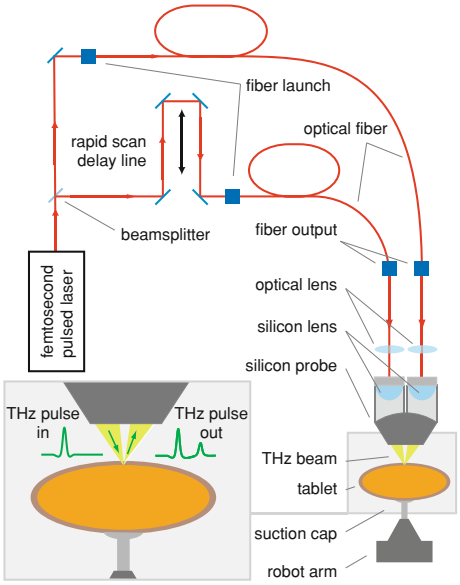

Fig. 18.6 Schematic diagram of a typical terahertz imaging setup used to image pharmaceutical tablets. The tablet samples are manipulated using a six-axis robotic arm. The system is capable of automatically point mapping over the entire surface of an arbitrarily shaped tablet. This configuration is utilised in the TPI imaga 2000 instrument by TeraView Ltd. (modified from [20])

optical excitation of a biased photoconductive antenna [77]. In this system terahertz pulses emitted from the photoconductive antenna are collimated and focused onto the sample using a silicon lens system. The reflected and backscattered terahertz pulses are then collected and focused, using the same silicon lens system, onto an unbiased photoconductive antenna for the laser-gated terahertz detection [78].

In TPI measurements, the transient electric field of the terahertz pulses is recorded as a function of the time delay between the terahertz pulse and the optical probe pulse. By sweeping the optical delay using a rapid variable delay stage, the entire terahertz waveform can be measured in less than 10 ms. As most pharmaceutical tablet excipients are transparent or semi-transparent to terahertz radiation, terahertz pulses incident on a tablet surface will penetrate through different coating layers. At each coating interface or abrupt change in refractive index (between drug particles and excipient matrix), a portion of the terahertz pulse is reflected back to the detector. This provides the contrast mechanism to map the drug and interfaces from different coating layers or subsurface structures within the tablet (Fig. 18.7).

To acquire a TPI map of a tablet terahertz waveforms are measured at 200 μm steps over the whole surface of a sample. Most pharmaceutical tablets have curved surfaces and, hence, a precise model of the surface shape and curvature of the tablet under investigation is the prerequisite for a reliable and quantitative TPI measurement. This surface model is obtained before the terahertz mapping step by using a laser gauge that uses a visible laser beam with a wavelength of 670 nm [20]. The model is generated automatically by moving the tablet in front of the laser gauge using the six-axis robot system. Once the topology model is acquired it can be used to present the tablet sample to the terahertz optics. During the entire TPI mapping step the tablet

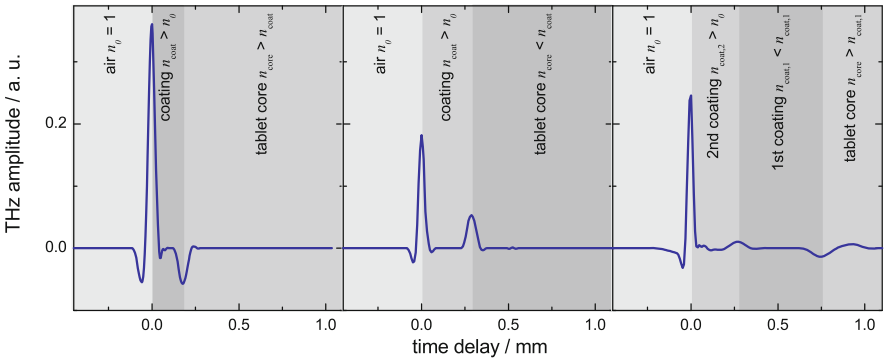

Fig. 18.7 Terahertz time-domain waveforms after signal processing of two samples of coated pharmaceutical tablets. The first two samples are coated with a single polymer layer. The *first reflection* is due to the interface between free space (air $n_0 = 1$) and the polymer coating. The *second reflection* originates from the interface between the polymer coating and the tablet core. In the sample on the *left* the refractive index on the coating material, n_{coat}, is higher than the refractive index of the tablet core, n_{core}, and hence a negative peak is observed. The opposite is the case for the sample in the centre. Here, $n_{\text{coat}} > n_{\text{core}}$, resulting in a second positive peak. In the third sample (*right*) there are two coating layers on top of one another with $n_{\text{coat},2} > n_{\text{coat},1} < n_{\text{core}}$

is kept precisely at the focal position with sample surface always perpendicular to the terahertz probe [79]. Consequently, no sample preparation is required and most pharmaceutical solid dosage forms with common shapes and surface curvatures can be directly imaged using this instrument [20].

In most imaging systems, in order to reduce the effects of water vapour absorption, the whole terahertz system and the sample under investigation have to be either purged with dry nitrogen gas or be evacuated throughout the measurement. However, this may not always be possible for some pharmaceutical solid dosage forms and is certainly not convenient for industry applications. By integrating both the THz emitter and detector into a specially designed silicon lens system (Fig. 18.6), the terahertz generation and detection are completely confined within the silicon lens system without any exposure of the terahertz pulse to the atmosphere before leaving the silicon optics. As the distance between the silicon lens and the sample is less than 8 mm, the effects of water vapour absorption on the terahertz waveform are minimal and no nitrogen purging is required, which greatly simplifies the measurements.

18.3.3 Signal Processing

The measured raw waveform is the convolution of the sample response and the system response of the instrument used as well as other effects such as systematic signal distortions, random noise and sample-structural effects.

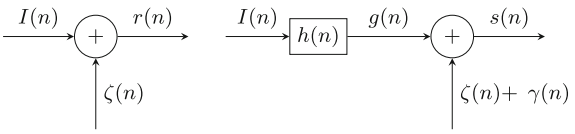

Fig. 18.8 Block diagram in problem definition without sample (*left*) and with sample (*right*). Adapted from [84]

Of these effects the systematic distortions are the most significant contributors to TPI measurement errors as they cause time delays, dispersion, phase change and after-runners in the THz pulse [80]. Causes of these distortions include reflections and subsidiary oscillations in the emitter; water molecule resonance absorption as THz radiation propagates through the system, and dispersive effects of the waveguides. Random noise includes emitter noise resulting from intensity fluctuations in the ultrafast laser, Johnson- Nyquist noise generated by charge carriers in the substrate in the absence of THz electrical field, thermal background radiation and more [81, 82]. Without proper modelling, structural effects of the sample cannot be quantified, adding to the complexity of signal analysis. These structural effects include back reflection and scattering effects. Back reflections are also known as parasitic reflections. Usually the intensity of this is insignificant compared to the fundamental reflections but it can become significant when there is a lamination problem in which an air gap is present between different layers of the sample [79]. Compared to imaging techniques utilising infrared or visible radiation TPI suffers from relatively less scattering effects as terahertz radiation wavelengths are significantly larger than most of the scattering structures of a sample [83]. However, scattering effects can become significant when there are a significant number of edges on the sample, such as embossing and breaking on pharmaceutical tablets or when the surface is very rough.

18.3.3.1 Definition of the Problem

The definition of the signal processing problem is modified from Refs. [84] and [85] under the assumption that the TPI measurement system is a linear time-invariant (LTI) system. Figure 18.8 shows the block diagram of a TPI system without and with the sample respectively. We refer to a sample as a particular point on the pharmaceutical tablet under examination, which will later contribute to a pixel of the terahertz image.

$r(n)$ is the TPI measurement in free space. Since the TPI measurement is based on reflection, $r(n)$ is obtained from a perfect terahertz reflection on a mirror. It is commonly known as the reference signal.

$$r(n) = I(n) + \zeta(n) \tag{18.2}$$

$I(n)$ is the input signal generated by the THz emitter. $\zeta(n)$ captures the background effects and corresponds to the detector reading before the emitter generates THz pulse. It is commonly known as the baseline signal. $\zeta(n)$ can be considered as additive

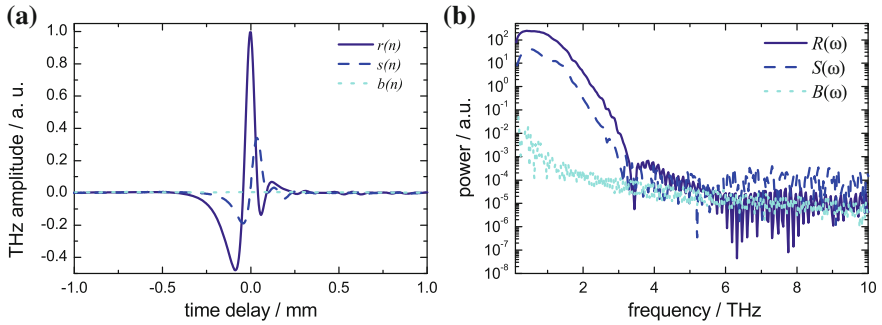

Fig. 18.9 Baseline, reference and raw sample signals in the: **a** time and **b** frequency domain

white Gaussian noise (AWGN), which is independently and identically distributed [86], and which is commonly referred to as the background signal.

A terahertz waveform comprises many time-discrete samples. Therefore, for theoretical clarity, the signal indices in the time domain are denoted by n instead of t in order to emphasise the discrete nature of TPI waveforms. The total number of data points, N, is large (usually $N = 512$), and hence the signals can be considered continuous in any mathematical operation.

When a sample is present in the TPI system, the resulting signal, also known as the sample signal $s(n)$ is:

$$s(n) = g(n) + \zeta(n) + \gamma(n) \tag{18.3}$$

$\zeta(n) + \gamma(n)$ is the system overall AWGN. $g(n)$ is the product of circular convolution (denoted by $\otimes$) of the input signal $I(n)$ and the original impulse response of the sample $h(n)$. Therefore, $s(n)$ can also be defined as:

$$s(n) = I(n) \otimes h(n) + \zeta(n) + \gamma(n) \tag{18.4}$$

Subsituting Eq. 18.2 into 18.4 leads to

$$s(n) - \zeta(n) = (r(n) - \zeta(n)) \otimes h(n) + \gamma(n) \tag{18.5}$$

The objective of signal processing is to obtain $\bar{h}(n)$ (the estimate of $h(n)$), given the baseline $\zeta(n)$, reference $r(n)$ and sample signals $s(n)$. This operation is generally known as deconvolution, as it is an attempt to extract $h(n)$ from the convolution $\otimes$. Figure 18.9 shows the baseline, reference and sample signals acquired from a pharmaceutical tablet.

Since $\zeta(n)$ is AWGN and not convoluted, it can be removed by simple subtraction. Eq. 18.5 now becomes:

$$s'(n) = r'(n) \otimes h(n) + \gamma(n) \tag{18.6}$$

where $s'(n)$ and $r'(n)$ are baseline-subtracted $s(n)$ and $r(n)$. Baseline subtraction is always the first and necessary step of signal processing. For notation simplicity, $s(n)$ and $r(n)$ should now be understood as $s'(n)$ and $r'(n)$. The overall AWGN of the system is always higher in the presence of the sample as compared to the baseline; this difference is represented by $\gamma(n)$ in Eq. 18.6 (Fig. 18.10).

18.3.3.2 Inverse Filtering

Conventionally, the estimated sample signal $\bar{h}(n)$ is obtained by dividing the raw signal $s(n)$ with the reference signal $r(n)$ in frequency domain:

$$\bar{h}(n) = \mathrm{FFT}^{-1}\left\{\frac{\mathrm{FFT}[s(n)]}{\mathrm{FFT}[r(n)]}\right\} \tag{18.7}$$

Equation 18.6 written in the frequency domain becomes

$$S(\omega) \approx R(\omega)H(\omega) + \Gamma(\omega) \tag{18.8}$$

The division between $S(\omega)$ and $R(\omega)$ is then

$$\bar{H}(\omega) \approx \frac{S(\omega)}{R(\omega)} = H(\omega) + \frac{\Gamma(\omega)}{R(\omega)} \tag{18.9}$$

Equation 18.9 shows that the division in the frequency domain amplifies any high frequency noise in the signal particularly when $|R(\omega)| \approx 0$ [85]. Coupling the frequency domain division with an appropriate band-pass filter, $f(n)$, can suppress these anomalies. The deconvolution now becomes [87]:

$$\bar{h}(n) = \mathrm{FFT}^{-1}\left\{\frac{\mathrm{FFT}[s(n)]}{\mathrm{FFT}[r(n)]}\mathrm{FFT}[f(n)]\right\} \tag{18.10}$$

This operation is generally known as inverse filtering. The band-pass filters that have been used in practice for terahertz signal deconvolution are the Double Gaussian (DG) and the Customised Skewed Gaussian (CSG) filters.

Double Gaussian filter

This is the most conventional filter used in TPI signal processing. Woodward et al. [88] and Pickwell et al. [89] used it to analyse TPI data for in vivo studies of human skin. As the name implies, it uses two Gaussian filters to act as high-pass and low-pass filters. The high-pass filter passes higher frequency components but attenuates lower frequency components. The opposite is true for low-pass filter. The time-domain DG filter is defined as:

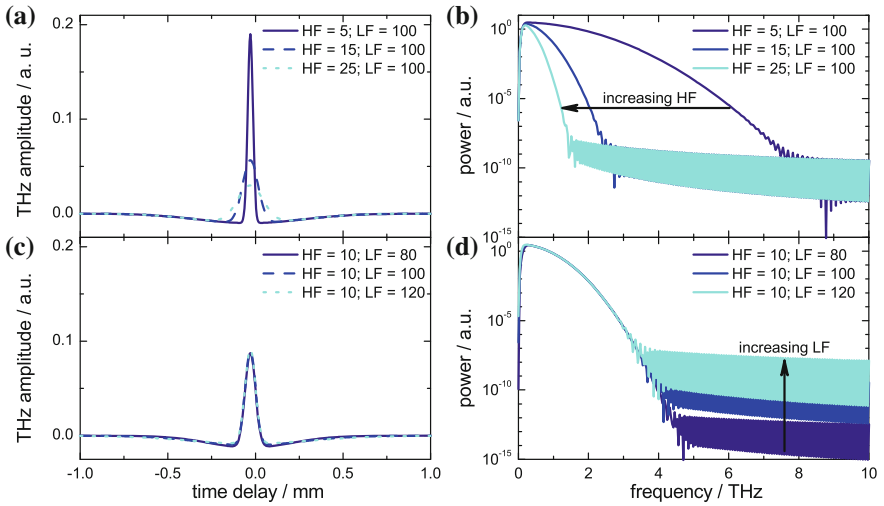

Fig. 18.10 The DG filter. Time-domain representations at different values of **a** HF and **c** LF; corresponding frequency-domain representations **b** HF and **d** LF

$$f_{\mathrm{DG}}(t) = \exp\left(-\frac{t^2}{\mathrm{HF}^2}\right) - \exp\left(-\frac{t^2}{\mathrm{LF}^2}\right) \tag{18.11}$$

where HF and LF define the pulse width of the high-pass and low-pass filters respectively.

At low LF, the shape of the deconvolved signals is distorted: it is difficult to differentiate between the interface peak and the deconvolution artefact, which emerges as two 'shoulders' at both ends of the surface peak (Fig. 18.11). Another type of artefact is the shifted signal 'tail' at high value of both HF and LF. At appropriate values of LF and HF, the deconvolution is satisfactory, resulting in deconvolved signals with distinguishable peaks and flat base.[1] In this acceptable parameter range, a lower value of HF and a higher value of LF improve the signal preservation due to an overall broader filter bandwidth, thus it is the best combination for the deconvolution.

Customised Skewed Gaussian Filter

In the context of TPI application in tablet coating analysis, the CSG is the most popular approach, as it is implemented in the commercial software package supplied by TeraView Ltd. The filter used in this method is a skewed DG filter customised to suit the application in tablet coating analysis. CSG is defined in time domain as:

[1] The signal base is the part of the signal that corresponds to terahertz wave propagation through the coating layer (between peaks) or deeper into the tablet matrix (after the last peak). Ideally, it should be flat so that peaks can be identified easily.

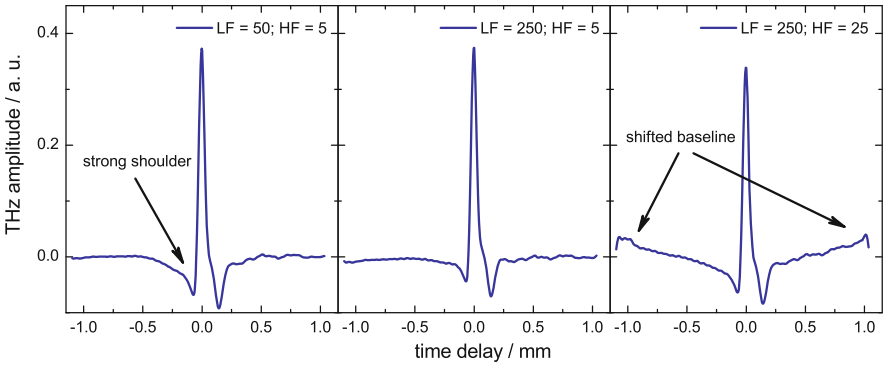

Fig. 18.11 DG inverse filter deconvolved signals at different values of HF and LF

$$f_{\mathrm{CSG}}(t) = \frac{1}{\sqrt{2\pi}} \exp\left[-\left(\frac{500t}{\mathrm{PW}}\right)^2\right] \tag{18.12}$$

where the PW corresponds to the pulse width of the Gaussian filter (Fig. 18.12).

Another important parameter of this method is the cut-off frequency (CF), which does not appear in the filter function but is incorporated in the deconvolution algorithm. As shown in Fig. 18.12b, it sets the frequency above which the high frequency components are removed from the frequency domain division (to prevent noise amplification as shown in Eq. 18.9). Figure 18.13 shows the effects of the different filter settings on a typical time-domain waveform.

18.3.4 Imaging of Pharmaceutical Tablets

18.3.4.1 General Principle

Figure 18.14a shows a typical terahertz time-domain waveform of a single pixel on a tablet which was coated with one polymer layer. The maximum at 0.00 mm is due to the reflection of terahertz pulse at the surface of the tablet, the interface between air and the coating.[2] The second peak at 0.38 mm is caused by the reflection of the terahertz pulse at the interface between coating and tablet core.

By plotting the mapped image points along one axis a B-scan (Fig. 18.14b) of the tablet can be obtained. This is a representation commonly used in ultrasonography or OCT. In this representation the curvature of the object is removed by projecting the image into a plane with all surface reflections lined up at $t = 0$ mm. This representation is useful to detect variations in coating thickness as well as density

[2] In all figures in this chapter the time delay is quoted in mm optical delay with $n_{\mathrm{air}} = 1$.

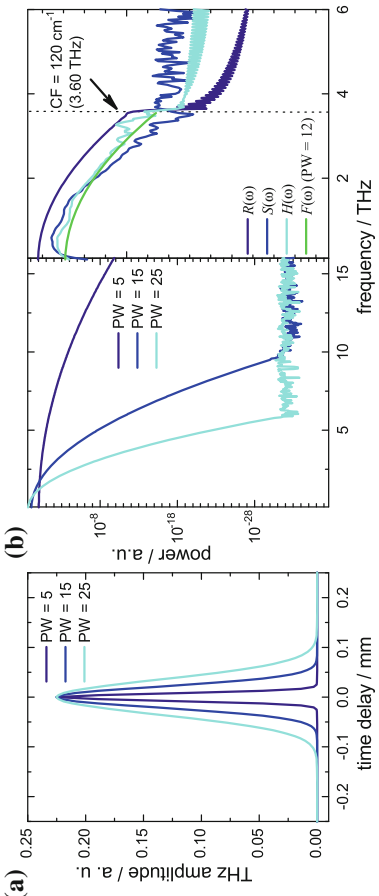

Fig. 18.12 The CSG filter. **a** Time-domain representations at different values of PW. **b** Corresponding frequency domain representations (*left*) and example for the implementation of the cut-off frequency, CF, during the signal processing in the frequency domain (*right*)

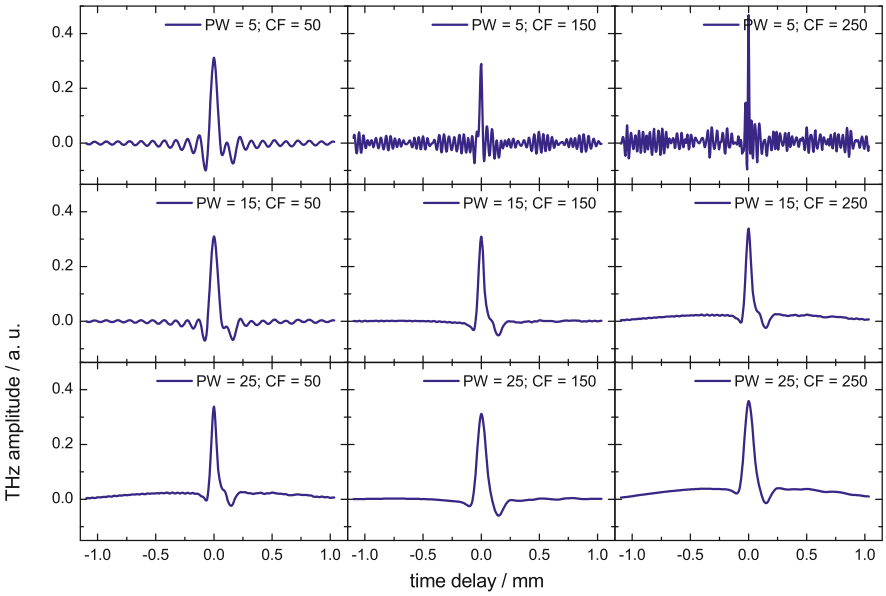

Fig. 18.13 CSG inverse filter deconvolved signals at different values of PW and CF. In this example the setting of PW = 15 and CF = 150 results in a good deconvolution

variations deeper in the tablet matrix. Alternatively, all pixels can be mapped out in a conventional 2D map (Fig. 18.14c).

Note that TPI is a 3D imaging technique and each TPI measurement provides a true 3D data cube: the x- and y-axes describe vertical and horizontal dimensions and the z-axis represents the time-delay dimension (depth-direction) of the sample. The lateral resolution is limited by the wavelength of the terahertz radiation and the depth resolution is limited by the pulse duration. For most pharmaceutical tablets, the achieved spatial resolution is typically in the range of 150–250 μm in lateral and 30–40 μm in axial direction [20, 79].

The surface topography model that was measured in the first step of the TPI measurement prior to acquiring the terahertz pulses as outlined in Sect. 18.3.2 is stored separately during the TPI measurement (Fig. 18.14d). This information can be combined with the 2D map to generate a 3D representation (Fig. 18.14e) and to extract tomographic slices from the data set (Fig. 18.14f).

18.3.4.2 Parameters

The most widely used application of TPI analysis of coated tablets is the non-destructive measurement of the coating thickness and its spatial distribution over the surface of the tablet. The coating thickness d can be directly extracted from the time-domain waveform:

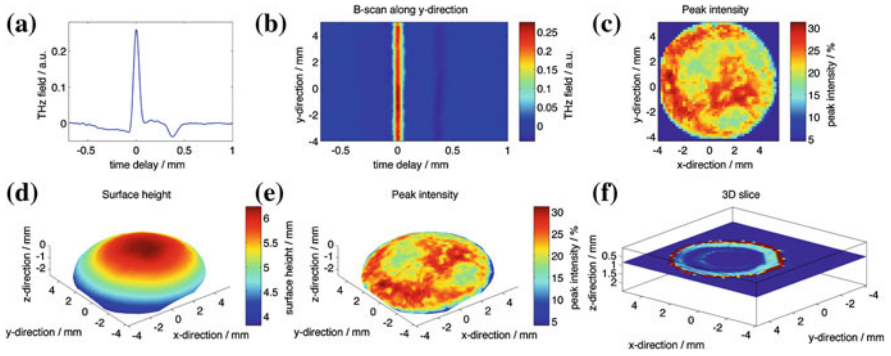

Fig. 18.14 Terahertz image of a single-layer coated tablet: **a** typical time-domain waveform of a single pixel; **b** B-scan map measured along the y-direction of the map at $x = 0$ mm. The *red line* at $t = 0$ mm represents the surface of the tablet while the subsequent *dark line* around $t = 0.40$ mm corresponds to the interface between the coating and the tablet core. **c** 2D map of all pixels acquired for one surface of the tablet. In this map the peak intensity (relative amplitude of the surface reflection compared to the amplitude of $r(n)$ is plotted). **d** Map of the surface height measured using the optical laser gauge; **e** 3D representation of the peak intensity map; and **f** 3D slice through the tablet

$$d = \frac{\Delta t c}{2n}, \tag{18.13}$$

where Δt is the time delay between the surface reflection and the reflection from the coating/core interface, c is the speed of light and n is the refractive index of the coating layer.

The refractive index of the coating layer can be measured by THz-TDS either using a free standing film of coating material which was cast out and dried or, if the tablet is sufficiently transparent, by directly using a coated tablet as a sample and an uncoated tablet core as a reference in a transmission measurement. Estimating the refractive index of the coating based on the volume fractions and the individual refractive indices of the different materials that make up the coating formulation is not recommended. As shown in Fig. 18.15 the TPI coating thickness measurements have been validated using X-ray microtomography as an independent technique on samples of the same tablets [90].

It is important to keep in mind that, while an accurate value for the refractive index is essential to obtain absolute coating thicknesses in most applications, it is the relative difference in coating thickness (for example the distribution of the film on the surface of a tablet or the relative differences in thickness between tablets of the same coating batch) that is of more interest.

Figure 18.16 shows images and histograms of the coating thickness distribution for a single-layer coated tablet. The big advantage of terahertz imaging is that the technique is capable of measuring not only an average coating thickness but also to resolve the homogeneity of the coating thickness across the entire surface of the tablet. Both the mean and the standard deviation of the coating thickness can be

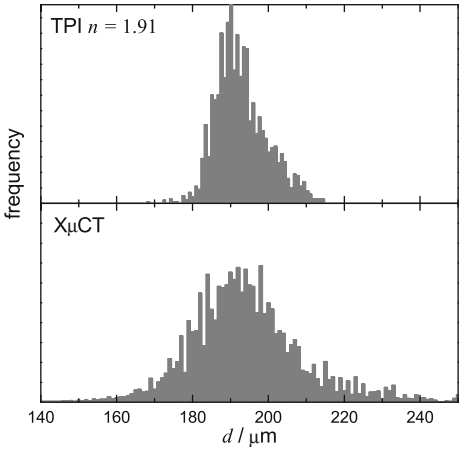

Fig. 18.15 Validation of the coating thickness measured by TPI using X-ray microtomography. For both measurements the same tablet was used. Very good agreement is found between the two techniques (modified from [90])

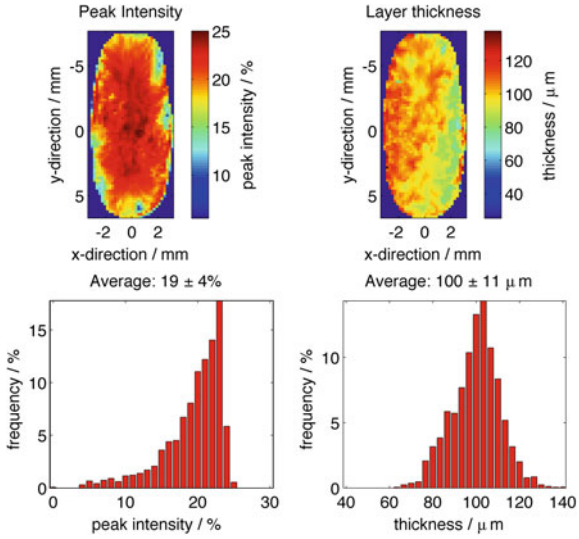

Fig. 18.16 False colour images and histograms of the peak intensity map (*left*), and the coating thickness distribution (*right*) for a single-layer coated tablet

measured non-destructively. In our example the histogram clearly indicates that the coating thickness over the entire surface of the tablet follows a normal distribution (Fig. 18.16); yet it is clear from the image that there is a distinctly thicker coating in the top left when compared to the bottom right. Such local variations in coating thickness are of no concern in a cosmetic coating, which is applied to give the tablet a uniform colour, gloss and visual appeal. However, if the coating is designed to control the drug release rate by means of a diffusion barrier, such local variation in coating thickness are critical as they will determine the overall diffusion rate of the tablet.

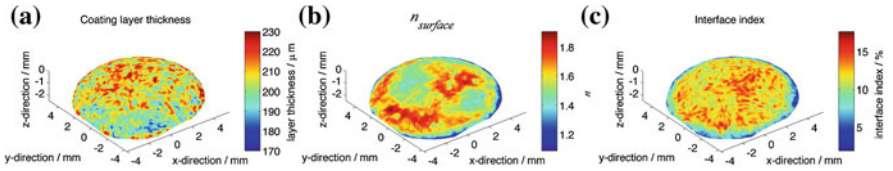

Fig. 18.17 Terahertz maps of **a** coating thickness, **b** surface refractive index, and **c** interface index. All maps show the same tablet in exactly the same orientation

In addition to the coating thickness (Fig. 18.17a) of a single layer, the waveform contains additional useful information: the amplitude of the first peak provides information on the refractive index at the tablet surface (Fig. 18.17b), which can be used to map out the tablet or coating hardness and/or density [91, 92]. Furthermore, it is possible to measure the coating thickness not only for the top layer but also for any subsequent layers which might be coated onto the tablet [20, 76].

A further property that can be extracted from the terahertz waveforms is the interface index, II, which is defined as

$$\mathrm{II} = \frac{|R_n|}{|R_0|}, \tag{18.14}$$

where R_n is the amplitude of the reflection at the nth interface and R_0 is the amplitude of the reflection from the surface of the sample. Figure 18.17c shows a map of the interface index.

18.3.5 Applications

18.3.5.1 Analysis of Tablet Coatings

As outlined in Sect. 18.3.1, coating of tablets with one or more polymer layers is a very common process step in pharmaceutical manufacturing. Traditionally, coatings were used merely for cosmetic purposes, to mask the taste of bitter drugs or to facilitate swallowing of the tablet. However, during the past decades functional coatings have become increasingly common. Functional coatings can be used to control the drug release site in the body as well as the release kinetics. A wide range of different types of coatings are used for this purpose. For example, enteric coatings, using polymers that are poorly soluble at low pH, are used to protect the drug molecules in the tablet against degradation in the acidic environment of the stomach; while sustained release coatings, where the polymer layer forms a porous diffusion barrier, are used to obtain a slow but sustained release profile. Typically, poorly soluble polymers across a broad range of pH are used for this purpose and the drug release kinetics is controlled by

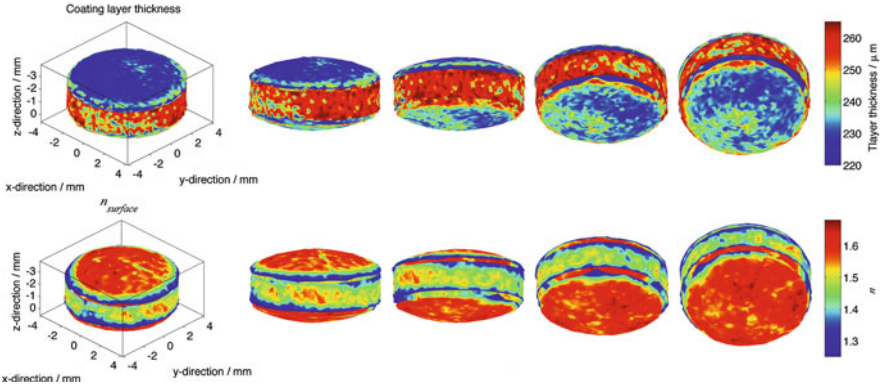

Fig. 18.18 3D maps of coating layer thickness (*top*) and surface refractive index (*bottom*) for a biconvex tablet

the polymer film thickness and its porosity. The quality of tablet coating will thus have direct implications on product performance [93].

In a proof-of-principle work, Fitzgerald et al. studied coated pharmaceutical tablets using a table-top flat-bed terahertz imaging system [76]. It was found that the coating thickness of sugar-coated tablets could be determined quantitatively and non-destructively. However, the coating thickness map obtained in this experiment only covered part of the tablet surface, as the samples had curved surfaces but acquisition was limited to a single xy plane. The success of this work led to the further development of commercial TPI instruments which were specifically designed for fully automated acquisition of terahertz images of arbitrarily shaped tablets as outlined in Sect. 18.3.2 [20, 79]. Using this instrument the coating thickness and uniformity could be readily obtained for a wide range of pharmaceutical dosage forms such as film-coated tablets, multi-layered controlled release tablets and soft gelatine capsules [20]. In other studies, TPI has been successfully applied for the analysis of coating thickness and uniformity of sustained release tablets [94], and for detecting weak spots in the coating that are not visible to the naked eye [95]. Malaterre et al. successfully applied TPI to investigate the coating characteristics of push–pull osmotic systems, a further controlled release tablet technology that is based on multiple coatings [96].

Because the TPI measurement covers the whole tablet surface, aspects of coating defects along with their site, depth and size can be identified using virtual terahertz cross-sections. Figure 18.18 shows a typical result for the intra-tablet variation in coating layer thickness for biconvex tablets, where the top and bottom surfaces of the tablet exhibit different coating characteristics to the centre band. In this example the coating thickness around the centre band of the tablet ($d = 255\,\mu$m) is thicker compared to the thickness of the the top and bottom surfaces and there is only a small difference in mean thickness between the top ($d = 227\,\mu$m) and bottom surfaces ($d = 236\,\mu$m).

Both cases, where the thickness of the centre band is thicker compared to the top and bottom surfaces as well as the opposite case, have been observed. Here, the density of the centre band was found to be lower compared to the top and bottom surfaces [97]. This difference in density is reflected in the lower refractive index of the surface of the polymer coating (Fig. 18.18). The results of the studies so far suggest that such variation in the microstructure of the coating is dependent on the process conditions during the coating operation. Factors such as tablet geometry, relative exposure to the spray zone and in particular the process scale, batch size and resulting pressure in the coating bed have been suggested to contribute to these findings. In general the effect seems more pronounced the smaller the process scale and batch size [94, 95]. The TPI results were confirmed by scanning electron microscopy (SEM) as well as by light microscopy on the same batch of tablets.

The standard quality control test for film coating is to determine the weight gain during coating by comparing the average mass of an uncoated tablet with that of a coated tablet. For this test it is assumed that the coating layer is uniformly distributed over the whole surface of the individual tablet and between all tablets of the same batch. However, the TPI results clearly demonstrated that this assumption is not always valid [94, 95].

One application of TPI coating measurements for which the measurement of the absolute layer thickness is critical is so-called active coating of tablets. In active coating a drug molecule (active pharmaceutical ingredient) is mixed into the soluble coating polymer. This layer typically contains a drug which is meant to be released quickly upon administration to the patient. In contrast, the tablet core might be a matrix formulation that will release further drug molecules slowly by diffusion once the active coating has disintegrated. Using such advanced drug delivery systems the drug release can be controlled very precisely and in turn the number of tablets the patient has to take per day can be reduced. For tablets with an active coating a uniform layer thickness throughout the production batch is extremely important as any deviation from the target thickness will either lead to too little drug in the tablet, which might not achieve the desired therapeutic effect, or more critically too high drug doses, which are toxic for the patient. Brock et al. have recently demonstrated a very good correlation between the coating thickness as measured by TPI and the drug content of the coated tablet as measured by high performance liquid chromatography after dissolving the same tablets (Fig. 18.19). TPI is unique in its quantitative ability to reliably measure the drug content even for very thick coating layers [98].

Another potential imaging method for coating analysis is OCT using near-infrared radiation [99, 100]. Zhong et al. reported experimental results of using OCT and TPI for quantitatively characterising pharmaceutical tablet coatings in the thickness range of 10–140 μm (Fig. 18.20) [101]. It was found that the OCT set-up for this application has an axial resolution of 0.9 μm, and is capable of quantifying thin coatings in the range of 10–60 μm. The maximum thickness of 60 μm that can be measured by OCT is limited by strong scattering of near-infrared light within the tablet coating and core due to its relatively short wavelength in the range of 0.5–1.0 μm. Terahertz radiation has a wavelength in the range of hundreds of microns, and thus TPI is much less affected by scattering limitations in this application. Using TPI it was

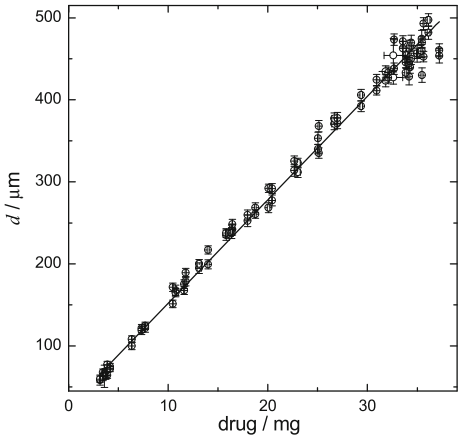

Fig. 18.19 Correlation between coating layer thickness as measured by TPI and the drug content in an active coating as measured subsequent by destructive chromatography (modified from [98])

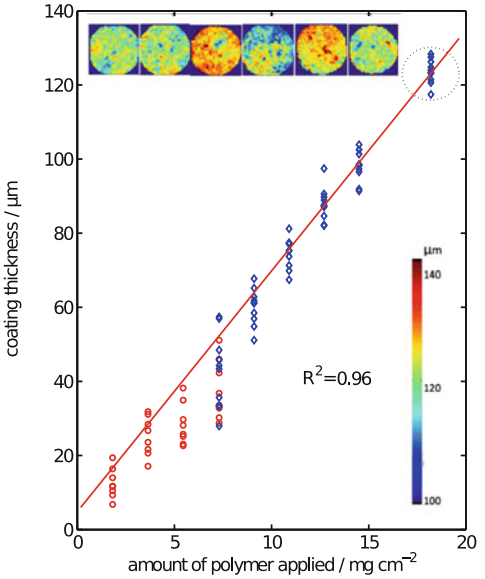

Fig. 18.20 The averaged coating thickness of individual tablets against the amount of polymer applied. The *diamonds* represent TPI results whilst the *circles* represent the OCT results; The *inset* shows TPI coating thickness maps (2D maps in xy directions) obtained for the tablets referring to the *circled data points* with a weight gain of 18.2 mg/cm^2. A large tablet-to-tablet variation of coating thickness is visible (modified from [101])

possible to measure thicker coatings in the range of 40–140 μm and beyond. The authors concluded that OCT and TPI are complementary analytical techniques for the non-destructive and quantitative characterisation of pharmaceutical tablet coatings [101]. OCT was better suited to resolve thin coatings which were below the resolution limit of TPI while TPI had clear advantages in analysing coating layers that were thicker than 60 μm.

18.3.5.2 Analysis and Monitoring of the Coating Process

TPI was used to monitor the progress of the coating process by offline analysis of samples that were removed at regular intervals from the tablet bed during film coating [102]. As expected, a linear correlation in coating thickness with the amount of applied polymer was found. In this study a sustained release coating was used and the authors found a linear correlation between the drug release and the coating thickness as measured by TPI. Scale-up of the process from the laboratory scale to the pilot scale resulted in a significant change in coating characteristics. The larger the process scale, the more dense the polymer film was found to be.

In two separate studies the results from TPI were compared with near-infrared (NIR) spectroscopy and imaging [103, 104]. Both TPI and NIR methods were able to measure the build-up of the coating layer as well as to detect small defects in the coating non-destructively. NIR imaging was found to be better at resolving thinner coating layers in the early stages of the coating process. It also has a higher spatial resolution compared with TPI. However, TPI has the advantage that its thickness measurements do not require further calibration even for very thick coating layers. This is in contrast to the NIR methods which always rely on thickness calibration by means of chemometric models that need to be specifically designed for each coating process.

This quality makes TPI interesting as a calibration tool for NIR and Raman measurements. Both techniques estimate the thickness of the coating based on the relative change in strength of spectral features. These spectral features are from chemicals that are either only found in the tablet core, in which case their attenuation indicates increasing coating thickness, or which are specific to the coating and hence stronger peaks relate to thicker coatings. The TPI measurements can thus be used to calibrate the NIR and Raman spectra for absolute coating thickness. In the example of an in-line Raman sensor Müller et al. demonstrated how a TPI calibration can be used to determine the endpoint of a coating process [105].

In a recent study, May et al. demonstrated for the first time how terahertz pulsed technology can be used to quantitatively measure the coating thickness of randomly moving tablets in a production scale pan coater using an in-line terahertz sensor (Fig. 18.21) [23]. The acquisition time to produce a coating thickness map of an entire tablet can be as much as 60 min using the TPI method outlined previously. In contrast the in-line sensor is able to assess the thickness of a single tablet in less than 9 ms during directly in the coater without interfering with the coating process. Direct thickness measurements of film coatings are achieved with sub-micron resolution without the need for any prior chemometric calibration models. Figure 18.22 shows a typical plot of coating thickness measured by the in-line process sensor as a function of process time. The ability to measure the coating thickness distribution in the coating pan in situ (Fig. 18.22b) cannot be achieved using any of the currently available near-infrared or Raman sensor technology, as each measurement point acquired with these techniques inherently represents the temporal and spatial average over a large number of tablets. The coating thickness distributions that are measured during the process clearly highlight the need for a better process understanding: while

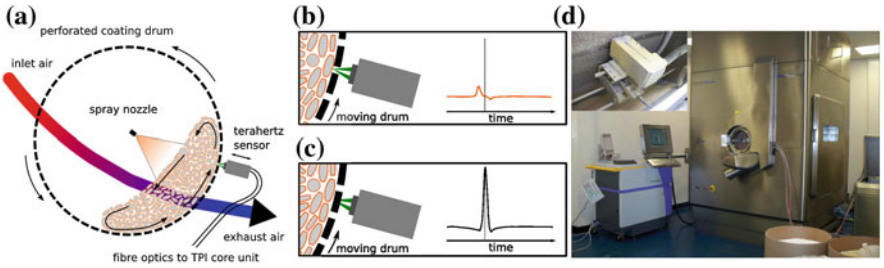

Fig. 18.21 Terahertz in-line sensor for coating thickness measurements. **a**, **c** Schematic of the sensor configuration; and **d** photograph of the sensor fitted into a production scale coater; the terahertz spectrometer on the *left* of the photograph is connected to the terahertz gauge using an optical fibre. The *inset* shows the terahertz sensor fitted behind the coating drum as outlined in (**a**) and (**b**) (modified from [23])

the measurement of the average coating thickness agrees well between the in-line and offline reference method, the in-line sensor reveals that there is a considerable population of tablets with much higher coating thickness in the coater that is not represented by the sample taken for offline analysis. In principle the in-line sensor allows terahertz technology to make their way from the development laboratory to the manufacturing floor. This exciting new sensor technology could have considerable impact in process understanding, process analytical technology (PAT) and quality-by-design (QbD) developments of film coating processes, although more research is required to assess its full potential.

18.3.5.3 Uncoated Tablets—Tablet Inspection and Solvent Diffusion

The ability of using TPI for the analysis of the "hardness" of pharmaceutical tablets was investigated by May et al. [92]. As shown in Fig. 18.23, radially symmetric spatial distributions in tablet density due to the shape of the punch used in the tablet manufacture were observed.

A strong correlation between the TPI results and those from diametric compression tests, the traditional destructive hardness test, was found and the TPI results were explained by means of finite element analysis (FEA) simulations. It was concluded that the TPI method is advantageous in that it is non-destructive in nature and at the same time provides additional information on the spatial distribution of the tensile strength of the tablet under study. This information can then be used to detect stresses originating from the compaction process that are buried under the surface of a tablet. Palermo et al. investigated the ability of TPI to quantitatively measure density maps of a tablet [91]. By using a multivariate calibration model, it was possible to predict the density of compacted mixtures of four excipients. Other studies [106, 107] indicate that TPI might also be useful for characterising tablet surface roughness and tablet bulk properties such as porosity non-destructively. More recently, Tuononen et

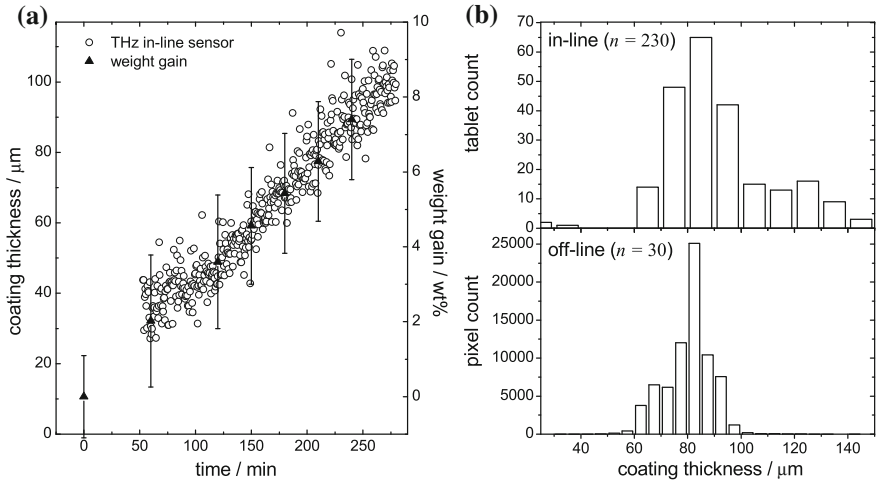

Fig. 18.22 Coating thickness measured by the in-line sensor: **a** coating thickness from 30 s averages as measured by the terahertz in-line sensor (*open circles*) and corresponding weight gain measurement (*filled triangles*); **b** variation in coating thickness of tablets sampled during 10 min process time using the in-line sensor (*top*) and from tablets removed at the same time using the offline TPI measurement. For the TPI measurement the histogram is plotted using all pixels from the images from all faces of the tablet (modified from [23])

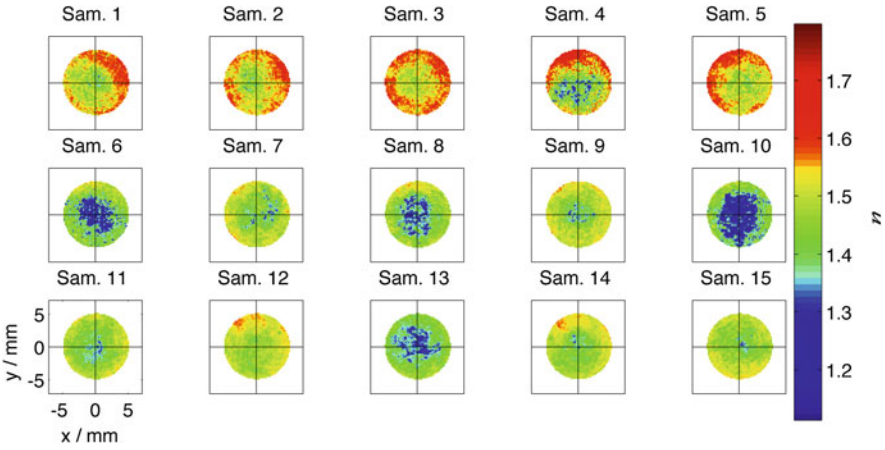

Fig. 18.23 Surface refractive index maps of 14 mm diameter, bi-convex tablets compressed at a compaction force of 8.87 kN (modified from [92])

al. showed that it was possible to estimate the real and imaginary part of the permittivity of the pure component of a starch acetate tablet [108]. All these results suggest that TPI is also suitable for the non-destructive analysis of uncoated pharmaceutical tablets. Other techniques such as X-ray computed tomography can also be used to

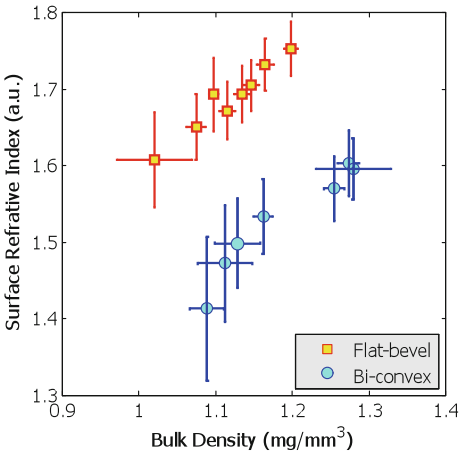

Fig. 18.24 Correlation between the surface refractive index and the bulk density of tablets of different geometry (modified from [92])

map the tablet density variation [109]. TPI has the additional advantage that terahertz radiation is non-ionising and hence inherently safe, which can be beneficial when it comes to industrial applications (Fig. 18.24).

Another area of interest for terahertz imaging is the study of solvent ingress into solid polymers. The topic is of great practical importance in the industry both with respect to the processing as well as the applications for polymers [110]. For certain applications (e.g. controlled drug delivery) solvent transport is desirable; however, in others, it causes degradation and contamination of the polymer (e.g. packaging) [111]. Accurate and time-resolved measurements of the liquid ingress process are very valuable for the validation of theoretical models of this process. The general measurement principle that terahertz technology can be used to study solvent diffusion processes into a polymer matrix was first demonstrated by Obradovic et al., as outlined in Sect. 18.2.3 [59]. In a related study, Portieri et al. investigated the hydration process of matrix tablets made from hydroxypropyl methylcellulose (HPMC) [112]. HPMC is a soluble polymer that is commonly used in the production of sustained release tablets. Once in contact with the dissolution medium the polymer swells and a layer of hydrogel is formed as a result of polymer hydration and chain relaxation. This layer then acts as a diffusion barrier for the subsequent release of drug molecules that are embedded in the polymer matrix. HPMC matrix tablets have become the model system to study this type of drug delivery system with a large range of experimental data as well as theoretical models published on this system [113, 114]. As shown in Fig. 18.25, initial experiments show that the shape and integrity of the gel layer formed after adding a 10 μl water drop onto an HPMC tablet can be mapped out using TPI. This information complements the results from other techniques such as magnetic resonance imaging [115] or infrared imaging [114].

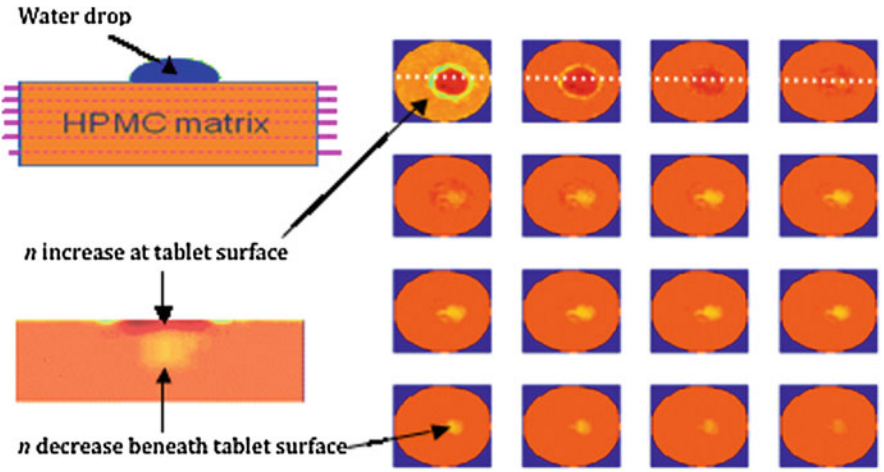

Fig. 18.25 Cross-sectional refractive index maps at various depths of 30 μm interval (*right*) and at $x = 0$ mm (*bottom-left*). Two distinct regions are clearly visible: a high-density shell (gel layer) at sample surface; and a low-density porous region (water channels) below the surface. The *white dotted line* in the figure (*right*) is where $x = 0$ mm, and the *red dotted lines* in the figure *inset* (*top-left*) represent various depths where cross-section maps were sliced

18.3.5.4 Dissolution Performance Prediction

The current regulatory framework in the pharmaceutical industry requires that a dissolution test of a small number of tablets ($n < 20$) is required by law to determine whether or not the quality of the entire batch ($n \gg 10^5$) is achieved and hence whether the product can be released to the market. A dissolution test works by exposing a tablet to a known quantity of dissolution medium (in the most simple case this is water) and by measuring how much drug is released from the tablet over time. This is done by taking samples of the liquid at regular intervals and subsequent analysis either by UV spectroscopy or liquid chromatography. This process, which can take up to 2 days for sustained release tablets, is very labour intensive and costly and has little statistical significance on the quality of the batch given the small sample size of tablets that are tested.

In a feasibility study, Spencer et al. demonstrated that the mean dissolution time (MDT) obtained using the standard dissolution test correlates with the coating thickness as measured by TPI [116]. In this study enteric coated tablets were investigated. This type of coating protects the drug molecules within the tablet from the acidic environment in the stomach, which is important for drug molecules that are unstable in such conditions or that would otherwise cause local irritations of the stomach. The coating is designed to remain intact at low pH and to dissolve quickly upon increasing the pH. It is not surprising that the correlation that was found by Spencer et al. was not very strong given that the coating thickness has no direct influence on the release rate as long as it remains intact at low pH. However, what is much more

important is that TPI was found to be a very powerful tool to ensure that no holes were present in the coating and that no drug is released at low pH, which is the main quality control concern in enteric coatings.

Following up from this study, Ho et al. investigated the potential of using terahertz data to predict the dissolution performance of coated sustained-release tablets where the thickness of the coating is expected to directly affect the drug release [97]. The correlation between coating thickness and MDT was very clear and much stronger than in the study by Spencer et al. In addition, the authors highlighted that changes in coating density, for instance as a result from scale-up, are also a good indicator for the dissolution performance of the coated tablet. In a further study by Ho et al., the whole terahertz waveforms, rather than the coating thickness and coating density alone, were used to predict the tablet dissolution performance [117]. Using a two-component PLS model, it was possible to predict the MDT for each tablet non-destructively. Such a multivariate method is particularly useful to predict the dissolution performance of tablets with very thin coatings, as currently the coating thickness below 30–40 μm cannot be determined by TPI.

Ho et al. also evaluated the applicability of TPI for the understanding of the process scale-up [102]. For this study a total of 190 sustained-release tablets that were sampled during the scale-up operation of a film coating process from the lab to the pilot scale were analysed by TPI and dissolution testing. Although the same mass of polymer was applied to all tablets the drug release from the tablets manufactured at pilot scale was significantly slower compared to the lab scale. The TPI results clearly revealed differences in coating thickness and density that explained these differences.

In a related study, the film coating thickness, drug layer uniformity and the effect of curing on the drug release from sustained-release coated pellets were investigated [118]. Pellets are spherical particles that are much smaller than tablets. They are typically used to fill capsules. Significant differences in film coating thickness, surface roughness and drug layer uniformity were found. No correlation between coating thickness and drug release was found. This was due to the fact that the solubility of the drug in the pellet core was very low and hence the release rate was limited by the drug solubility rather than the diffusion rate through the coating. The pellets used in this study (5 mm) were much larger in diameter compared to the dimensions of the pellets typically used in the industry ($<$1 mm). The large diameter was chosen to allow measurements using the TPI system. Future experiments will have to show whether smaller particles can be reliably measured using terahertz imaging and whether such measurements are practical and quantitative.

All the studies show that TPI has an excellent sensitivity with which to assess the coating quality of pharmaceutical tablets. A clear correlation of the TPI results to dissolution performance was found. The speed and ease of TPI mapping may make it an attractive non-destructive alternative for dissolution testing both in product development and with the potential to play a significant role to improve the product safety by increasing the number of tablets that are tested to a statistically meaningful level in the quality control of the end product. However, it was highlighted that TPI can only predict the dissolution behaviour if the coating is the rate determining

factor of the drug delivery system and that other parameters need also to be taken into account.

18.3.5.5 Chemical Mapping

Given the sensitivity of terahertz radiation to the intermolecular interactions in typical drug molecules as outlined in Chap. 8, chemical mapping is an exciting extension of the structural imaging outlined before for the characterisation of complex heterogeneous samples. The basis of chemical mapping is the acquisition of a 3D data set where two axes describe vertical and horizontal spatial dimensions and the third axis represents the spectral frequency dimension. As previously discussed, the electric field of terahertz radiation is recorded as a function of time in a TPI measurement. The spectral information of this signal can be obtained by Fourier transformation. The absorption coefficient, $\alpha(\nu)$, and the refractive index, $n(\nu)$, are then calculated for each pixel as [79]:

$$n(\nu) + j\frac{\alpha(\nu)c}{4\pi\nu} = \frac{1 - S(\nu)/R(\nu)}{1 + S(\nu)/R(\nu)} \tag{18.15}$$

where $S(\nu)$ and $R(\nu)$ are the Fourier transforms of the measured terahertz waveforms reflected from a sample and a reference mirror. The absorption spectra $\alpha(\nu)$ provide means for chemical mapping of pharmaceutical solid dosage forms [34, 119]. Note that a transmission configuration, rather than the reflection geometry as discussed in this section, can also be used for chemical sensing and imaging [19, 120].

In the near-infrared and mid-infrared range, FTIR and Raman spectroscopy have been successfully developed for chemical mapping [121–123]. However, many pharmaceutical tablet coatings are opaque to infrared radiation, owing to either strong absorption or scattering. Therefore, conventional infrared techniques are most suitable for mapping out the surface distributions of chemicals as a 2D chemical mapping technique. In addition, near-infrared and mid-infrared imaging technology sometimes struggles to discriminate between pharmaceutical polymorphs as such polymorphs often only differ by subtle shifts in their respective vibrational spectra. Terahertz radiation, on the other hand, can penetrate much deeper into a tablet. At the same time it is very sensitive to subtle changes in crystal structure [124–126]. Therefore, in principle, TPI provides the necessary penetration depth and spectral specificity for non-destructive chemical mapping in a 3D matrix.

Using a model tablet sample that contained well-confined domains of lactose and tartaric acid, Shen et al. demonstrated how the spectral signature of the materials could indeed be extracted non-destructively at depth [35]. A time-partitioned Fourier transform of the reflected terahertz waveform with a fixed window width was employed to produce depth-resolved spectral components of the pulse [35, 79]. There are many potential applications for this technique in the context of pharmaceutical dosage forms such as investigating the spatial distribution of different polymorphic forms in a dosage form. Changes in the crystal structure of the drug can be induced

during manufacture of the dosage form by compaction or coating or by moisture uptake during storage of a tablet [8]. However, it is important to mention that the model tablet used [35, 79] was made of polyethylene, which is almost transparent to terahertz radiation. For a realistic pharmaceutical tablet, the spectral resolution at depth will be influenced strongly by scattering and refraction caused by the tablet matrix. Further work will be necessary to develop a robust method to routinely perform 3D chemical mapping experiments. In addition, most commercial TPI systems provide a lateral resolution of around 200 μm and better resolution is necessary in order to resolve small polymorph/hydrate particles within pharmaceutical dosage forms.

18.3.5.6 Summary of Pharmaceutical Applications

Over the past five years, terahertz technology was developed into a new tool for the physical characterisation of solid dosage forms in the pharmaceutical industry. Located in the far-infrared region of the electromagnetic spectrum, terahertz spectra directly probe intermolecular vibrations such as phonon lattice modes of crystalline solids. This gives terahertz spectroscopy a high sensitivity for the rapid discrimination and quantification of polymorphs, hydrates, cocrystals and other solid-state modifications of drug molecules as well as for the analysis of solid form transformation dynamics [33, 124, 127–130]. On the other hand, terahertz radiation can penetrate deep into pharmaceutical tablets as most common pharmaceutical excipients are amorphous and semi-transparent to terahertz radiation. As summarised in this section, this can be exploited in TPI as a powerful tool for the non-destructive and quantitative characterisation of coatings on tablets.

18.4 Outlook

A number of properties make terahertz radiation very attractive for industrial applications: it can penetrate deep into a wide range of technical materials such as polymers, ceramics and semiconductors. The low photon energy gives terahertz radiation an inherent safety advantage compared to X-ray techniques, and, compared to other well-established NDT such as ultrasonics, terahertz radiation has higher resolution to offer while completely avoiding coupling problems from free space given the low refractive index mismatch. At the same time the measurements reveal a wealth of information on the microstructure of the materials probed, including the internal structure, defects, density gradients, moisture content and intermolecular interaction.

However, to live up to this enormous potential, there are a number of challenges that terahertz sensors have to master. First and foremost the technology has to become faster, more stable and more affordable, which requires new approaches to many details of the terahertz system architecture. The current laser stability, the overall instrument reliability, together with the requirement of regular service visits in order

to maintain the instrument performance, are huge obstacles that need to be addressed. In addition, it would be desirable to extend the spectral range of the current instruments from $100\,\mathrm{cm}^{-1}$ to, for example $300\,\mathrm{cm}^{-1}$. This would allow the terahertz spectrum to cover both the intermolecular and some of the intramolecular vibration modes, thus providing better spectral specificity for a larger range of materials. The broader spectral range would also help to characterise thinner layer structures with higher spatial resolution. On the signal processing side there are still a number of open questions, such as how to best account for scattering losses from sharp edges in terahertz images as well as how best to reconstruct volumetric tomographic data sets while taking refraction into account quantitativey. Moreover, advances in both software and hardware have to be made to make this technology accessible in non-specialist communities.

In this chapter we have highlighted a range of what we believe to be very promising applications, ranging from industrial sensors for in-line control of a production line in polymer composite processing to fault detection in semiconductors and tablet inspection in the pharmaceutical industry amongst others. Terahertz technology has the potential to play a significant role in all these areas.

Acknowledgments The authors would like to thank Ms. Bee Yin Yeo for her help in putting together Sect. 18.3.3 of this chapter.

References

1. B. Hu, M. Nuss, Opt. Lett. **20**(16), 1716 (1995)
2. D. Mittleman, R. Jacobsen, M.C. Nuss, IEEE J. Sel. Top. Quantum Electron. **2**(3), 679 (1996)
3. D. Mittleman, S. Hunsche, L. Boivin, M. Nuss, Opt. Lett. **22**(12), 904 (1997)
4. D. Mittleman, M. Gupta, R. Neelamani, R. Baraniuk, J. Rudd, M. Koch, Appl. Phys. B Lasers Opt. **68**(6), 1085 (1999)
5. J.B. Jackson, M. Mourou, J. Labaune, J.F. Whitaker, I.N.I. Duling, S.L. Williamson, C. Lavier, M. Menu, G.A. Mourou, Meas. Sci. Technol. **20**(7), 075502–075511 (2009)
6. C. Jansen, S. Wietzke, O. Peters, M. Scheller, N. Vieweg, M. Salhi, N. Krumbholz, C. Jördens, T. Hochrein, M. Koch, Appl. Opt. **49**(19), E48 (2010)
7. J.A. Zeitler, P.F. Taday, D.A. Newnham, M. Pepper, K.C. Gordon, T. Rades, J. Pharm. Pharmacol. **59**(2), 209 (2007)
8. J.A. Zeitler, L.F. Gladden, Eur. J. Pharm. Biopharm. **71**(1), 2 (2009)
9. Y.C. Shen, Int. J. Pharm. **417**, 48 (2011)
10. B. Ferguson, X. Zhang, Nat. Mater. **1**(1), 26 (2002)
11. D. Mittleman (ed.), *Sensing with Terahertz Radiation*. Springer Series in Optical Sciences Series, (Springer, Berlin, 2003)
12. K. Kawase, Opt. Photonics News **15**(10), 34 (2004)
13. W. Chan, J. Deibel, D. Mittleman, Rep. Prog. Phys. **70**(8), 1325 (2007)
14. M. Tonouchi, Nat. Photonics **1**(2), 97 (2007)
15. S. Dexheimer (ed.), *Terahertz Spectroscopy: Principles and Applications*. Optical Science and Engineering, (CRC Press, Boca Raton, 2007)
16. I. Duling, D. Zimdars, Nat. Photonics **3**, 630 (2009)
17. Y.S. Lee, *Principles of Terahertz Science and Technology* (Springer, New York, 2009)
18. P.U. Jepsen, D.G. Cooke, M. Koch, Laser Photonics Rev. **5**(1), 124 (2010)

19. M. Walther, B.M. Fischer, A. Ortner, A. Bitzer, A. Thoman, H. Helm, Anal. Bioanal. Chem. **397**(3), 1009 (2010)
20. J.A. Zeitler, Y. Shen, C. Baker, P.F. Taday, M. Pepper, T. Rades, J. Pharm Sci. **96**(2), 330 (2007)
21. N. Krumbholz, T. Hochrein, N. Vieweg, T. Hasek, K. Kretschmer, M. Bastian, M. Mikulics, M. Koch, Polym. Testing **28**(1), 30 (2009)
22. D. Zimdars, I. Duling, G. Fichter, J. White, AIP Conf. Proc. **1211**(1), 564 (2010)
23. R.K. May, M.J. Evans, S. Zhong, I. Warr, L.F. Gladden, Y. Shen, J.A. Zeitler, J. Pharm Sci. **100**(4), 1535 (2011)
24. L. Cartz, *Nondestructive testing* (ASM International Materials Park, Ohio, 1995)
25. C. Hellier, *Handbook of nondestructive evaluation* (McGraw-Hill, New York, 2001)
26. M. Soleimani, R. Bayford, Philos. Trans. R. Soc. A Math. Phys. Eng. Sci. **367**(1900), 3017 (2009)
27. D. Ensminger, L. Bond, Ultrasonics: fundamentals, technologies and applications, 3rd edn. Mechanical Engineering, (Taylor and Francis, Boca Raton, 2009)
28. D. Stifter, Appl. Phys. B Lasers Opt. **88**(3), 337 (2007)
29. I. Pupeza, R. Wilk, M. Koch, Opt. Express **15**(7), 4335 (2007)
30. R. Wilk, I. Pupeza, R. Cernat, M. Koch, I. Pupeza, R. Cernat, IEEE J. Sel. Top. Quant. Electron. **14**(2), 392 (2008)
31. M. Walther, B. Fischer, P.U. Jepsen, Chem. Phys. **288**(2–3), 261 (2003)
32. B. Fischer, M. Hoffmann, H. Helm, R. Wilk, F. Rutz, T. Kleine-Ostmann, M. Koch, P. Jepsen, Opt. Express **13**(14), 5205 (2005)
33. C.J. Strachan, T. Rades, D.A. Newnham, K.C. Gordon, M. Pepper, P.F. Taday, Chem. Phys. Lett. **390**(1–3), 20 (2004)
34. Y. Shen, P.F. Taday, D.A. Newnham, M. Pepper, Semicond. Sci. Tech. **20**(7), S254 (2005)
35. Y. Shen, P.F. Taday, D.A. Newnham, M. Kemp, M. Pepper, R. Hwu, K. Linden, *Terahertz and Gigahertz Electronics and Photonics IV* (SPIE Press, California, 2005), pp. 24–31
36. K. Yamamoto, M. Yamaguchi, M. Tani, M. Hangyo, S. Teramura, T. Isu, N. Tomita, Appl. Phys. Lett. **85**(22), 5194 (2004)
37. D. Banerjee, W. von Spiegel, M. Thomson, S. Schabel, H. Roskos, Opt. Express **16**(12), 9060 (2008)
38. H. Zhang, K. Mitobe, N. Yoshimura, in *International Symposium on Electrical Insulating Materials (ISEIM)*, (IEEE, 2008), pp. 87–90
39. P. Parasoglou, E.P.J. Parrott, J.A. Zeitler, J. Rasburn, H. Powell, L.F. Gladden, M.L. Johns, Terahertz Sci. Technol. **3**, 172 (2010)
40. R. Cunnell, T. Luce, J. Collins, R. Rungsawang, J. Freeman, H. Beere, D.A. Ritchie, L.F. Gladden, M.L. Johns, J.A. Zeitler, in *34th International Conference on Infrared, Millimeter, and Terahertz Waves*, IRMMW-THz 2009 (IEEE, 2009), pp. 1–2
41. E.P.J. Parrott, J.A. Zeitler, J. McGregor, S. Oei, H. Unalan, S. Tan, W. Milne, J. Tessonier, R. Schlogl, L.F. Gladden, J. Phys. Chem. C **113**(24), 10554 (2009)
42. J. McGregor, Z. Huang, E.P.J. Parrott, J.A. Zeitler, K. Nguyen, J. Rawson, A. Carley, T. Hansen, J.P. Tessonnier, D. Su, D. Teschner, E. Vass, A. Knop-Gericke, R. Schlögl, L.F. Gladden, J. Catal. **269**(2), 329 (2010)
43. M. de Silva, C. McElroy, J. McGregor, A. York, J.A. Zeitler, L.F. Gladden, in *35th International Conference on Infrared Millimeter and Terahertz Waves (IRMMW-THz)*, (2010), pp. 1–2
44. R. Arrigo, M. Havecker, S. Wrabetz, R. Blume, M. Lerch, J. McGregor, E.P.J. Parrott, J.A. Zeitler, L.F. Gladden, A. Knop-Gericke, R. Schlögl, D. Su, J. Am. Chem. Soc. (2010)
45. C. Jördens, M. Koch, Opt. Eng. 47(3), 037003 (2008)
46. D. Zimdars, J. Valdmanis, J. White, G. Stuk, S. Williamson, W. Winfree, E. Madaras, in *AIP Conference Proceedings*, (2005), pp. 570–577
47. H. Zhong, J. Xu, X. Xie, T. Yuan, R. Reightler, E. Madaras, X. Zhang, IEEE Sens. J. **5**(2), 203 (2005)
48. R.F. Anastasi, E.I. Madaras, J.P. Seebo, S.W. Smith, J.K. Lomness, P.E. Hintze, C.C. Kammerer, W.P. Winfree, R.W. Russell, in *Proceedings of the SPIE*, (2007), pp. 1–6

49. D. Zimdars, G. Fichter, A. Chernovsky, in *33rd International Conference on Infrared, Millimeter and Terahertz Waves (IRMMW-THz 2008)* (IEEE, 2008), pp. 1–3
50. Y. Morita, A. Dobroiu, K. Kawase, C. Otani, Opt. Eng. **44**(1), (2005)
51. Y. Morita, A. Dobroiu, C. Otani, K. Kawase, J. Food Prot. **68**(4), 833 (2005)
52. C. Jördens, M. Scheller, S. Wietzke, D. Romeike, C. Jansen, T. Zentgraf, K. Wiesauer, V. Reisecker, M. Koch, Compos. Sci. Technol **70**(3), 472 (2010)
53. D. Zimdars, J. White, G. Fichter, A. Chernovsky, S.L. Williamson, Proc. SPIE **6949**(1), 69490B (2008)
54. C. Chen, D. Lee, T. Pollock, J. Whitaker, Opt. Express **18**(4), 3477 (2010)
55. P. Lopato, T. Chady, R. Sikora, Int. J. Comput. Math. Electr. Electron. Eng. (COMPEL) **30**(4), 1260 (2011)
56. D.K. Hsu, K.H. Im, C.P. Chiou, D.J. Barnard, AIP Conf. Proc. **1335**(1), 533 (2011)
57. Y. Cai, Z. Wang, R. Dias, D. Goyal, in *Proceedings of the 60th Electronic Components and Technology Conference (ECTC)* (2010), pp. 1309–1315
58. J.M. Chin, V. Narang, X. Zhao, M.Y. Tay, A. Phoa, V. Ravikumar, L.H. Ei, S.H. Lim, C.W. Teo, S. Zulkifli, M.C. Ong, M.C. Tan, Microelectron. Reliab. **51**(9–11), 1440 (2011)
59. J. Obradovic, J. Collins, O. Hirsch, M.D. Mantle, M.L. Johns, L.F. Gladden, Polymer **48**(12), 3494 (2007)
60. Q. Wu, T. Hewitt, X. Zhang, Appl. Phys. Lett. **69**(8), 1026 (1996)
61. Z. Jiang, X. Zhang, Opt. Lett. **23**(14), 1114 (1998)
62. M. Usami, T. Iwamoto, R. Fukasawa, M. Tani, M. Watanabe, K. Sakai, Phys. Med. Biol. **47**(21), 3749 (2002)
63. M. Yamashita, M. Usami, K. Fukushima, R. Fukasawa, C. Otani, K. Kawase, Appl. Opt. **44**(25), 5198 (2005)
64. M. Usami, M. Yamashita, K. Fukushima, C. Otani, K. Kawase, Appl. Phys. Lett. **86**(14), 3 (2005)
65. T. Yasuda, T. Yasui, T. Araki, E. Abraham, Opt. Commun. **267**(1), 128 (2006)
66. T. Yasuda, Y. Kawada, H. Toyoda, H. Takahashi, Opt. Express **15**(23), 15583 (2007)
67. A. Lee, Q. Hu, Opt. Lett. **30**(19), 2563 (2005)
68. R. Kohler, A. Tredicucci, F. Beltram, H. Beere, E.H. Linfield, A. Davies, D.A. Ritchie, R. Iotti, F. Rossi, Nature **417**(6885), 156 (2002)
69. A.W.M. Lee, B.S. Wil, S. Kumar, Q. Hu, J.L. Reno, IEEE Photon. Technol. Lett. **18**(13), 1415 (2006)
70. P. Dean, N.K. Saat, S.P. Khanna, M. Salih, A. Burnett, J. Cunningham, E.H. Linfield, A.G. Davies, Opt. Express **17**(23), 20631 (2009)
71. K. Nguyen, M.L. Johns, L.F. Gladden, C. Worrall, P. Alexander, H. Beere, M. Pepper, D.A. Ritchie, J. Alton, S. Barbieri, E.H. Linfield, Opt. Express **14**(6), 2123 (2006)
72. F. Clarke, Vib. Spectrosc. **34**(1), 25 (2004)
73. V. Busignies, B. Leclerc, P. Porion, P. Evesque, G. Couarraze, P. Tchoreloff, Eur. J. Pharm. Biopharm. **64**(1), 38 (2006)
74. J. Aaltonen, K.C. Gordon, C.J. Strachan, T. Rades, Int. J. Pharm. **364**(2), 159 (2008)
75. C. McGoverin, T. Rades, K.C. Gordon, J. Pharm Sci. **97**(11), 4598 (2008)
76. A.J. Fitzgerald, B.E. Cole, P.F. Taday, J. Pharm Sci. **94**(1), 177 (2005)
77. D. Auston, Appl. Phys. Lett. **26**(3), 101 (1975)
78. D. Auston, K. Cheung, P. Smith, Appl. Phys. Lett. **45**(3), 284 (1984)
79. Y. Shen, P.F. Taday, IEEE J. Sel. Top. Quantum Electron. **14**(2), 407 (2008)
80. J.R. Fletcher, G.P. Swift, D. Dai, J.M. Chamberlain, P.C. Upadhya, J. Appl. Phys. **102**(11), 113105 (2007)
81. W. Withayachumnankul, H. Lin, S. Mickan, B. Fischer, D. Abbott, in *Photonic Materials, Devices, and Applications II* (Maspalomas, Gran Canaria, 2007)
82. W. Withayachumnankul, B. Fischer, H. Lin, D. Abbott, J. Opt. Soc. Am. B **25**(6), 1059 (2008)
83. V. Wallace, P.F. Taday, A.J. Fitzgerald, R. Woodward, J. Cluff, R. Pye, D.A. Arnone, Faraday Discuss. **126**, 255 (2004)
84. B. Ferguson, D. Abbott, Microelectr. J. **32**(12), 943 (2001)

85. R. Neelamani, H. Choi, R. Baraniuk, IEEE Trans. Signal Process. **52**(2), 418 (2004)
86. D.L. Donoho, IEEE Trans. Inf. Theory **41**(3), 613 (1995)
87. Y. Chen, S. Huang, E. Pickwell-Macpherson, Opt. Express **18**(2), 1177 (2010)
88. R. Woodward, B. Cole, V. Wallace, R. Pye, D.A. Arnone, E.H. Linfield, M. Pepper, Phys. Med. Biol. **47**(21), 3853 (2002)
89. E. Pickwell, B.E. Cole, A.J. Fitzgerald, M. Pepper, V.P. Wallace, Phys. Med. Biol. **49**(9), 1595 (2004)
90. I. Russe, D. Brock, K. Knop, P. Kleinbudde, J.A. Zeitler, in *8th World Meeting on Pharmaceutics, Biopharmaceutics and Pharmaceutical Technology* (Istanbul, 2012), p. 2
91. R. Palermo, R. Cogdill, S. Short, J. Drennen Iii, P. Taday, J. Pharma. Biomed. **46**(1), 36 (2008)
92. R. May, L. Han, J. Alton, S. Zhong, J. Elliott, C. Byers, L. Gladden, M. Evans, Y. Shen, J. Zeitler, in *34th International Conference on Infrared, Millimeter, and Terahertz Waves*, IRMMW-THz 2009 (IEEE, 2009), pp. 1–2
93. G.M. Jantzen, J.R. Robinson, in *Modern pharmaceutics*, ed. by C.T. Rhodes, G.S. Banker (CRC Press, New York, 2002), pp. 501–528
94. L. Ho, R. Mueller, M. Romer, K.C. Gordon, J. Heinamaki, P. Kleinebudde, M. Pepper, T. Rades, Y.C. Shen, C.J. Strachan, P.F. Taday, J.A. Zeitler, J. Controlled Release **119**(3), 253 (2007)
95. L. Ho, R. Mueller, C. Krueger, K.C. Gordon, P. Kleinebudde, M. Pepper, T. Rades, Y. Shen, P.F. Taday, J.A. Zeitler, J. Pharm. Sci. **99**(1), 392 (2010)
96. V. Malaterre, M. Pedersen, J. Ogorka, R. Gurny, N. Loggia, P. Taday, Eur. J. Pharm. Biopharm. **74**(1), 21 (2009)
97. L. Ho, R. Mueller, K.C. Gordon, P. Kleinebudde, M. Pepper, T. Rades, Y. Shen, P.F. Taday, J.A. Zeitler, J. Controlled Release **127**(1), 79 (2008)
98. D. Brock, J.A. Zeitler, A.Funke, K. Knop, P. Kleinebudde, submitted to Int. J. Pharm. (2012)
99. S. Zhong, H. Shen, Y.C. Shen, J.A. Zeitler, L. Ho, M. Evans, P. Taday, M. Pepper, T. Rades, K.C. Gordon, R. Muller, P. Kleinebudde, in *34th International Conference on Infrared, Millimeter, and Terahertz Waves*, IRMMW-THz 2009 (IEEE, 2009), pp. 1–2
100. J.M.A. Mauritz, R.S. Morrisby, R.S. Hutton, C.H. Legge, C.F. Kaminski, J. Pharm. Sci. **99**(1), 385 (2010)
101. S. Zhong, Y.C. Shen, L. Ho, R.K. May, J.A. Zeitler, M. Evans, P.F. Taday, M. Pepper, T. Rades, K.C. Gordon, R. Mueller, P. Kleinebudde, Opt. Laser Eng. **49**(3), 361 (2011)
102. L. Ho, R. Mueller, K.C. Gordon, P. Kleinebudde, M. Pepper, T. Rades, Y. Shen, P.F. Taday, J.A. Zeitler, Eur. J. Pharm. Biopharm. **71**(1), 117 (2009)
103. R. Cogdill, R. Forcht, Y. Shen, P. Taday, J. Pharm. Innov. (2), 29 (2007)
104. L. Maurer, H. Leuenberger, Int. J. Pharm. **370**(1–2), 8 (2009)
105. J. Müller, D. Brock, K. Knop, J.A. Zeitler, P. Kleinebudde, Eur. J. Pharm. Biopharm. 80, 690–697 (2012)
106. M. Juuti, H. Tuononen, T. Prykäri, V. Kontturi, M. Kuosmanen, E. Alarousu, J. Ketolainen, R. Myllylä, K.-E. Peiponen, Meas. Sci. Technol. (1), 015301 (2009)
107. H. Tuononen, E. Gornov, J.A. Zeitler, J. Aaltonen, K.-E. Peiponen, Opt. Lett. **35**(5), 631 (2010)
108. H. Tuononen, K. Fukunaga, M. Kuosmanen, J. Ketolainen, K.-E. Peiponen, Appl. Spectrosc. **64**(1), 127 (2010)
109. I. Sinka, S. Burch, J. Tweed, J. Cunningham, Int. J. Pharm. **271**(1–2), 215 (2004)
110. T. Hyde, L. Gladden, Polymer **39**(4), 811 (1998)
111. S.G. Harding, M.L. Johns, S.R. Pugh, P.J. Fryer, L.F. Gladden, Food Addit. Contam. **14**(6–7), 583 (2012)
112. A. Portieri, P.F. Taday, Y.C. Shen, in *58th Pittsburgh Conference on Analytical and Applied Spectroscopy*, (PITTCON 2007) (Chicago, USA, 2007)
113. J. Siepmann, Adv. Drug Deliv. Rev. **48**(2–3), 139 (2001)
114. S. Kazarian, K. Chan, Macromolecules **36**(26), 9866 (2003)
115. Y.Y. Chen, Hughes, L. P., L.F. Gladden, M.D. Mantle, J. Pharm Sci. **99**(8), 3462 (2010)

116. J. Spencer, Z. Gao, T. Moore, L. Buhse, P.F. Taday, D.A. Newnham, Y. Shen, A. Portieri, A. Husain, J. Pharm. Sci. **97**(4), 1543 (2008)
117. L. Ho, R. Mueller, K.C. Gordon, P. Kleinebudde, M. Pepper, T. Rades, Y. Shen, P.F. Taday, J.A. Zeitler, J. Pharm. Sci. **98**(12), 4866 (2009)
118. L. Ho, Y. Cuppok, S. Muschert, K. Gordon, M. Pepper, Y. Shen, F. Siepmann, J. Siepmann, P. Taday, T. Rades, Int. J. Pharm. **382**(1–2), 151 (2009)
119. R. Cogdill, S. Short, R. Forcht, Z. Shi, Y. Shen, P. Taday, C. Anderson, J. Drennen, J. Pharm. Innov. **1**(1), 63 (2006)
120. B. Fischer, M. Hoffmann, H. Helm, G. Modjesch, P.U. Jepsen, Semicond. Sci. Tech. **20**(7), S246 (2005)
121. E.N. Lewis, P.J. Treado, R.C. Reeder, G.M. Story, A.E. Dowrey, C. Marcott, I.W. Levin, Anal. Chem. **67**(19), 3377 (2012)
122. J.L. Koenig, S.Q. Wang, R. Bhargava, Anal. Chem. **73**(13), 360A (2001)
123. F.C. Clarke, M.J. Jamieson, D.A. Clark, S.V. Hammond, R.D. Jee, A.C. Moffat, Anal. Chem. **73**(10), 2213 (2001)
124. J.A. Zeitler, D.A. Newnham, P.F. Taday, T.L. Threlfall, R.W. Lancaster, R.W. Berg, C.J. Strachan, M. Pepper, K.C. Gordon, T. Rades, J. Pharm. Sci. **95**(11), 2486 (2006)
125. E.P.J. Parrott, J.A. Zeitler, T. Friscic, M. Pepper, W. Jones, G.M. Day, L.F. Gladden, Cryst. Growth Des. **9**(3), 1452 (2009)
126. R. Li, J.A. Zeitler, D. Tomerini, E.P.J. Parrott, L.F. Gladden, G.M. Day, Phys. Chem. Chem. Phys. **12**(20), 5329 (2010)
127. P.F. Taday, I. Bradley, D.A. Arnone, M. Pepper, J. Pharm. Sci. **92**(4), 831 (2003)
128. C.J. Strachan, P.F. Taday, D.A. Newnham, K.C. Gordon, J.A. Zeitler, M. Pepper, T. Rades, J. Pharm. Sci. **94**(4), 837 (2005)
129. J.A. Zeitler, D.A. Newnham, P.F. Taday, C.J. Strachan, M. Pepper, K.C. Gordon, T. Rades, Thermochim. Acta **436**(1–2), 71 (2005)
130. J.A. Zeitler, K. Kogermann, J. Rantanen, T. Rades, P.F. Taday, M. Pepper, J. Aaltonen, C.J. Strachan, Int. J. Pharm. **334**(1–2), 78 (2007)